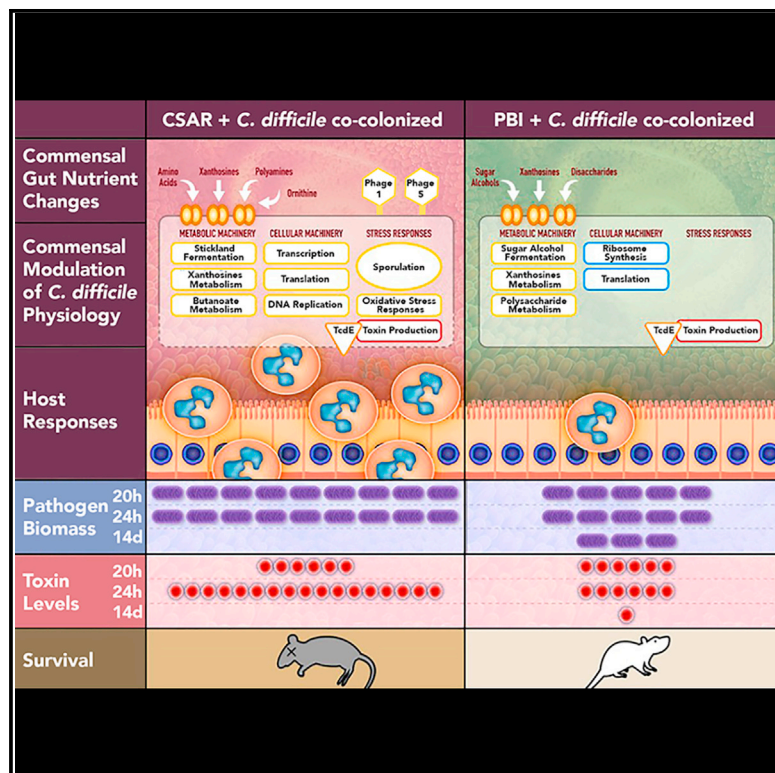


Cell Host & Microbe

In vivo commensal control of *Clostridioides difficile* virulence

Graphical abstract



Authors

Brintha P. Girinathan,
Nicholas DiBenedetto,
Jay N. Worley, ..., Nitin S. Baliga,
Bruno Dupuy, Lynn Bry

Correspondence

lbry@bwh.harvard.edu

In brief

Girinathan et al. define complex mechanisms by which individual gut commensals limit or worsen *Clostridioides difficile* pathogenicity. Integrated, high-resolution analyses of metabolomic, metatranscriptomic and phenotypic outcomes identify complex intermicrobe interactions *in vivo* to delineate how commensals uniquely shape the intestinal environment to impact microbial programs, which may enlighten bacteriotherapeutic approaches.

Highlights

- Systems biology models identify complex host and inter-microbe interactions *in vivo*
- *P. bifementans* alone protects the murine host against lethal *C. difficile* disease
- *C. sardiniense* worsens disease through cross-feeding and growth enhancement
- Findings inform successful bacteriotherapeutic development against *C. difficile*



Article

In vivo commensal control of *Clostridioides difficile* virulence

Brintha P. Girinathan,^{1,10,11} Nicholas DiBenedetto,^{1,10,12} Jay N. Worley,^{1,2} Johann Peltier,^{3,4} Mario L. Arrieta-Ortiz,⁵ Selva Rupa Christinal Immanuel,⁵ Richard Lavin,^{1,12} Mary L. Delaney,^{1,6} Christopher K. Cummins,¹ Maria Hoffman,⁷ Yan Luo,⁷ Narjol Gonzalez-Escalona,⁷ Marc Allard,⁷ Andrew B. Onderdonk,^{1,6} Georg K. Gerber,^{1,8} Abraham L. Sonenshein,⁹ Nitin S. Baliga,⁵ Bruno Dupuy,³ and Lynn Bry^{1,6,13,*}

¹Massachusetts Host-Microbiome Center, Brigham & Women's Hospital, Harvard Medical School, Boston, MA 02115, USA

²National Center of Biotechnology Information, National Library of Medicine, Bethesda, MD 20894, USA

³Laboratoire Pathogenèse des Bactéries Anaérobies, Institut Pasteur, UMR CNRS 2001, Université de Paris, 25-28 Rue du Dr. Roux, Institut Pasteur, 75015 Paris Cedex, France

⁴Institute for Integrative Biology of the Cell (I2BC), CEA, CNRS, Université Paris-Saclay, 91198, Gif-sur-yvette Cedex, France

⁵Institute for Systems Biology, Seattle, WA 98109, USA

⁶Clinical Microbiology Laboratory, Department of Pathology, Brigham & Women's Hospital, Boston, MA 02115, USA

⁷Center for Food Safety and Applied Nutrition, United States Food and Drug Administration, Department of Microbiology, College Park, MD 20740, USA

⁸Harvard-MIT Health Sciences & Technology, Cambridge, MA 02139, USA

⁹Department of Molecular Biology and Microbiology, Tufts University School of Medicine, Boston, MA 02111, USA

¹⁰These authors contributed equally

¹¹Present address: Ginkgo Bioworks, Cambridge, MA 02210, USA

¹²Present address: Department of Molecular Biology and Microbiology, Tufts University School of Medicine, Boston, MA 02111, USA

¹³Lead contact

*Correspondence: lbry@bwh.harvard.edu

<https://doi.org/10.1016/j.chom.2021.09.007>

SUMMARY

Leveraging systems biology approaches, we illustrate how metabolically distinct species of *Clostridia* protect against or worsen *Clostridioides difficile* infection in mice by modulating the pathogen's colonization, growth, and virulence to impact host survival. Gnotobiotic mice colonized with the amino acid fermenter *Paraclostridium bifermentans* survive infection with reduced disease severity, while mice colonized with the butyrate-producer, *Clostridium sardiniense*, succumb more rapidly. Systematic *in vivo* analyses revealed how each commensal alters the gut-nutrient environment to modulate the pathogen's metabolism, gene regulatory networks, and toxin production. Oral administration of *P. bifermentans* rescues conventional, clindamycin-treated mice from lethal *C. difficile* infection in a manner similar to that of monocolonized animals, thereby supporting the therapeutic potential of this commensal species. Our findings lay the foundation for mechanistically informed therapies to counter *C. difficile* disease using systems biology approaches to define host-commensal-pathogen interactions *in vivo*.

INTRODUCTION

Clostridioides difficile infections cause substantial morbidity and mortality (Allegretti et al., 2019; Worley et al., 2020). Fecal microbiota transplant (FMT) has become standard of care for recurrent infections by reconstituting a protective microbiota (Leslie et al., 2019). Mechanisms of commensal protection have included conversion of host-primary to -secondary bile acids, which inhibit *C. difficile* spore germination (Buffie et al., 2015), production of antimicrobial peptides (Mills et al., 2018; Valdés-Varela et al., 2016; Zheng et al., 2018), and a promiscuous commensal bacteriophage that can disrupt pathogen growth (Baktash et al., 2018). However, we know little about the molecular mechanisms by which specific microbes modulate the pathogen's virulence *in vivo*. Given FMT-related deaths in immunocompromised pa-

tients (Marcella et al., 2021), therapies informed by molecular mechanisms of action will enable options with improved safety and efficacy.

C. difficile's pathogenicity locus (PaLoc) contains the TcdA and TcdB toxins and TcdE holin involved in toxin release. TcdR encodes a sigma factor specific for the toxin gene promoters (Bouillaut et al., 2015; Mani and Dupuy, 2001). *In vivo*, *C. difficile*, like other cluster XI *Clostridia*, utilizes diverse carbon sources including carbohydrates, amino acids fermented via Stickland reactions, and ethanolamine (Dubois et al., 2016). Stickland metabolism can drive rapid pathogen growth, particularly with abundant proline, glycine, or leucine, which serve as electron acceptors for the *prd*, *grd*, and *had* enzyme systems, respectively (Bouillaut et al., 2015; Hofmann et al., 2018; Neumann-Schaal et al., 2015). The pathogen also fixes carbon



through the Wood-Ljungdhal pathway to generate acetate for metabolism (Nawrocki et al., 2018; Neumann-Schaal et al., 2019). *C. difficile*'s conditional regulatory networks closely integrate its cellular metabolism and virulence programs, particularly through the CodY and CcpA metabolic repressors that repress PaLoc expression under nutrient sufficiency (Martin-Verstraete et al., 2016) and promote toxin expression with starvation to extract nutrients from the host. CodY and CcpA coregulate additional gene systems in cellular metabolism, sporulation, and stress responses by sensing host and commensally produced factors including inflammatory ROS and antimicrobial peptides (Kint et al., 2017; Neumann-Schaal et al., 2018).

Host and microbiota can thus influence the pathogen's virulence via multiple mechanisms. Among Stickland-fermenting cluster XI Clostridia, *Paraclostridium bifermentans* preferentially uses Stickland fermentations for energy. In contrast, *Clostridium sardiniense*, a glycolytic cluster I species, produces abundant butyrate through anaerobic carbohydrate fermentation (Moore, 1993). Both species colonize the human gut yet have very different metabolic capabilities.

Using defined colonization and infection experiments in gnotobiotic mice (Reeves et al., 2012; Wilson et al., 1986) with Environmental and Gene Regulatory Influence Network (EGRIN) and Phenotype of Regulatory Influences integrated with Metabolism and Environment (PRIME) models of *C. difficile*'s conditional regulatory networks (Arrieta-Ortiz et al., 2021), we show how individual species of commensal *Clostridia* affect host survival of *C. difficile* infection, at the level of the microbial pathways and small molecules that modulate *C. difficile*'s regulatory networks to drive pathogen growth and virulence. Findings promoted development of a defined bacteriotherapeutic able to rescue an infected conventional host from lethal infection. By defining how individual commensals systematically modulate *C. difficile*'s physiology, we enable mechanistically informed approaches for this disease.

RESULTS

Single commensals dramatically alter host outcomes from *C. difficile* infection

C. difficile infection in 6-week-old germ-free mice caused rapid demise (Figures 1A and 1B). Symptoms developed at 20 h post-challenge with weight loss and diarrhea. Animals demonstrated focal epithelial damage with neutrophilic infiltrates at 24 h (Figure 1C versus 1D) that by 32 h showed widespread erosions and worsening symptomatic disease.

In contrast, mice precolonized with *P. bifermentans* prior to *C. difficile* challenge survived (Figure 1B; $p < 0.0001$) with milder symptoms and colonic damage (Figure 1E versus 1D). Fourteen days post-infection, animals regained lost weight and demonstrated intact intestinal epithelium with lymphocytic infiltrates having replaced acute neutrophilic infiltrates (Figure 1F).

Mice precolonized with *C. sardiniense* developed more rapidly lethal infection (Figure 1B; $p < 0.0001$), with epithelial sloughing and neutrophils entering the lumen at 20 h of infection (Figure 1G) followed by widespread mucosal denudation and rapid demise (Figure 1H).

Toxin levels (Figure 1I) at 20 h, the first point of symptoms, were comparable among cohorts although pathogen vegetative and spore biomass in *C. sardiniense* co-colonized mice were 3-fold

higher (Figures 1J and 1K). However, by 24 h *C. difficile* mono-colonized and *C. sardiniense* co-colonized mice demonstrated 2 to 3-fold higher toxin levels, vegetative biomass, and neutrophilic infiltrates than *P. bifermentans* co-colonized mice (Figures 1I and 1J). After 14 days, toxin levels in surviving *P. bifermentans* co-colonized mice fell >80% from acute levels (Figure 1I).

While *C. sardiniense* biomass rose 10-fold in *C. difficile*-infected mice, *P. bifermentans* biomass did not change acutely. Commensal colonization also did not alter toxin integrity or cytotoxic activity (Figures 1L and 1M).

Commensals condition the gut-nutrient environment prior to *C. difficile*'s introduction

Given commensal effects on pathogen biomass, carbon-source enrichment analyses of the gut-metabolomic environment evaluated the nutrient content available for *C. difficile* growth and metabolism (Figures 2A and 2B).

Germ-free cecal contents were enriched for multiple classes of carbohydrates (Figures 2A and 2C) including hexoses, pentoses, and sugar alcohols of dietary origin that have poor absorption from the gut (Pruss and Sonnenburg, 2021; Theriot et al., 2014). Gut contents were also enriched for multiple fermentable amino acids (Figures 2D and 2E), including the Stickland-acceptor amino acid proline (Figure 2E), and multiple purines and pyrimidines (Figures 2A and 2F). In the absence of colonizing microbiota, SCFA were not detected (Figure 2G).

Colonization with *C. sardiniense* or with *P. bifermentans* markedly altered luminal conditions prior to *C. difficile*'s introduction. *C. sardiniense* monocolonization enriched multiple amine-containing carbon sources (Figure 2A, top) including Stickland-fermentable amino acids (Figures 2D and 2E), γ -glutamyl amino acids (Griffith et al., 1979), and polyamines. Branched-chain amino acids increased 2 to 3-fold (Figure 2D) and ornithine >16-fold over germ-free levels (Figure 2E).

C. sardiniense depleted luminal fructose, left mannitol and sorbitol unchanged, and enriched amino sugars, including those originating from host glycoconjugates (Figure 2C). *C. sardiniense* monocolonization produced >5-fold increases in hypoxanthines and metabolites produced by other purinolytic *Clostridia* (Bradshaw, 1960) (Figure 2F) and > 10-fold increases in the uracil metabolites 3-ureidopropionate and beta-alanine (Vogels and Van der Drift, 1976) (Figure 2F). The SCFA fermentation metabolites acetate and butyrate were produced (Figure 2G).

In contrast, *P. bifermentans* monocolonization depleted polyamines and Stickland acceptor and other fermentable amino acids (Figure 2A, middle), consuming > 70% of proline, > 50% of glycine, > 50% of threonine, and 80% of 4-hydroxyproline, a host collagen-degradation product, which many Stickland fermenters convert to proline (Figure 2E) (Huang et al., 2018). *P. bifermentans* produced abundant 5-aminovaleate (Figure 2H) from proline, isocaproate from reductive leucine Stickland metabolism (Kim et al., 2006), and isobutyrate, isovalerate, and 2-methylbutyrate from Stickland oxidative fermentation of branched-chain amino acids (Figure 2G). Stickland aromatic amino acid metabolites including 3-phenylpropionate from phenylalanine, 3-(4-hydroxy-phenylpropionate) from tyrosine, and indole lactate from tryptophan were also produced (Figure 2I).

P. bifermentans consumed > 50% of fructose, left sugar-alcohol levels unchanged (Figure 2C) and produced acetate and

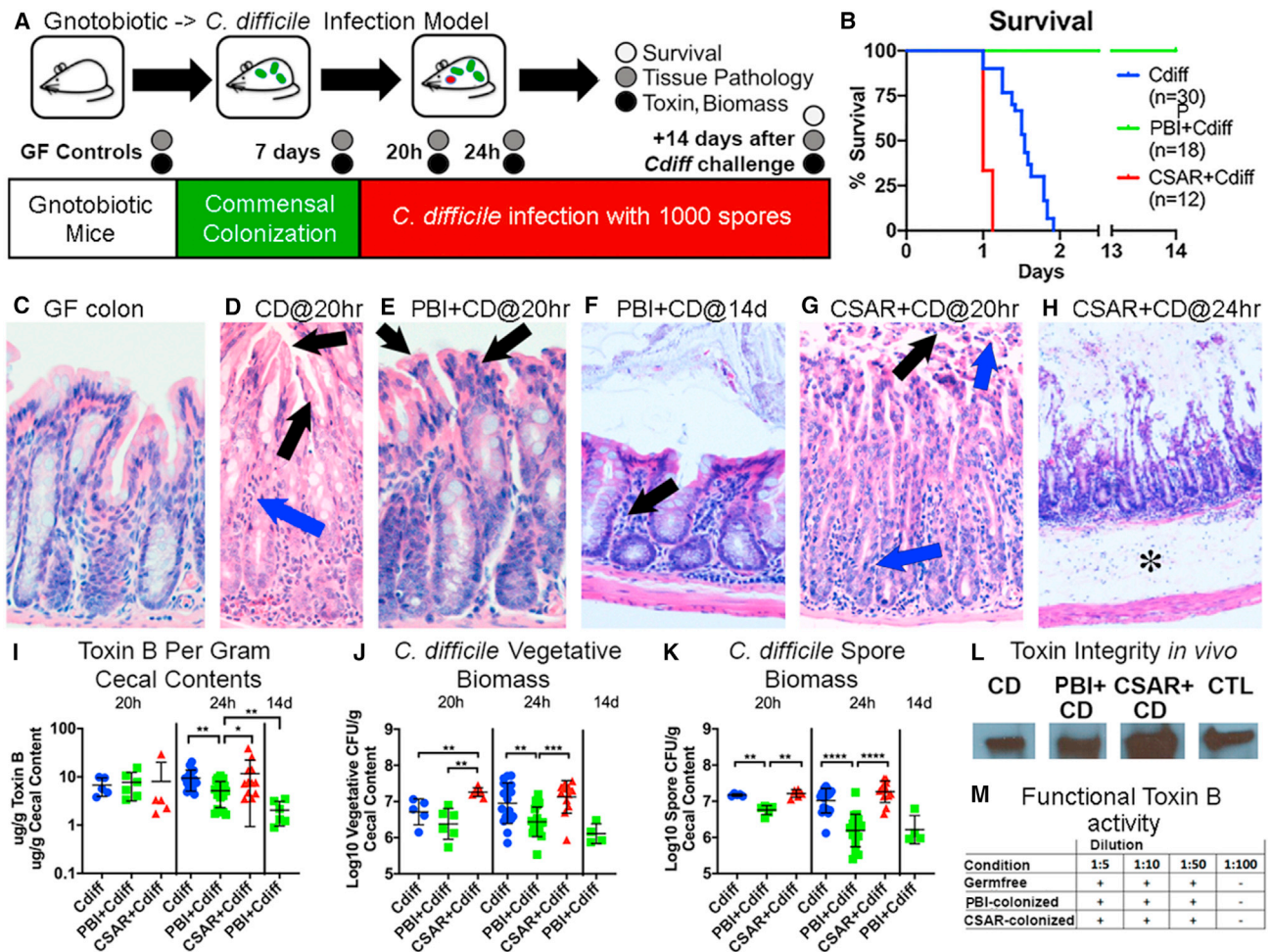


Figure 1. *P. biferrmentans* protects germ-free mice from lethal *C. difficile* infection while *C. sardiniense* promotes more severe disease

(A) Experimental overview.
 (B) Survival curves.
 (C–H) Colonic hematoxylin and eosin (H&E) stains. Magnification: 200× (C–E); 100× (F and G); and 40× (H).
 (C) Normal germ-free mucosa.
 (D) *C. difficile*-infected mice at 20 h, showing epithelial stranding and vacuolation (black arrows) and neutrophil infiltrates (blue arrow).
 (E) *P. biferrmentans* co-colonized mice at 20 h of infection showing vacuolization of apical colonocytes (black arrows) but nominal inflammation.
 (F) *P. biferrmentans*- and *C. difficile*-infected mice at 14 days showing intact epithelium and lymphocytic infiltrates (black arrow).
 (G) *C. sardiniense*- and *C. difficile*-infected mice at 20 h of infection showing surface epithelial loss and pseudomembrane formation (black arrow) and transmural neutrophilic infiltrates entering the lumen (blue arrows).
 (H) *C. sardiniense* co-colonized mice at 24 h of infection showing epithelial denudation and severe submucosal edema (asterisk).
 (I) Log₁₀ of extracellular cecal ToxinB (μg/g). Bars show mean and standard deviation. Mann-Whitney significance values: *0.01 < p ≤ 0.05; **0.001 < p ≤ 0.01; ***0.0001 < p ≤ 0.001; ****p ≤ 0.0001.
 (J) Log₁₀ *C. difficile* vegetative CFU. Bars show mean and standard deviation.
 (K) Spore biomass per gram of cecal contents. Bars show mean and standard deviation.
 (L) Western blot of cecal contents showing intact toxinB in *C. difficile* (CD) infected, *P. biferrmentans* + *C. difficile*, or *C. sardiniense* + *C. difficile* co-colonized mice. (CTL, control toxinB). (M) Effects of GF, *P. biferrmentans*, or *C. sardiniense*-monocolonized cecal contents on the toxicity of exogenously added toxinB. No differences were noted in toxinB cytopathic effect against human fibroblasts. See Figure S1.

propionate (Figure 2G). *P. biferrmentans* monocolonization enriched hypoxanthines (Figure 2F). 3-ureidopropionate increased to a lesser extent than in *C. sardiniense*-monocolonized mice and without increased beta-alanine (Figure 2F).

C. difficile monocolonized mice demonstrated the broadest depletion of carbohydrate and amine-containing carbon sources (Figure 2A, bottom). The pathogen-depleted Stick-

land-acceptor amino acids consuming > 50% of glycine, > 70% of proline, and > 85% of 4-hydroxyproline (Figure 2E), with a concomitant increase in 5-aminovalerate (Figure 2H); γ-glutamyl amino acids, other fermentable amino acids (including cysteine and threonine), and N-acetyl conjugates of proline, branched-chain amino acids, and polyamines were also depleted. Hexoses, pentoses, and sugar alcohols were

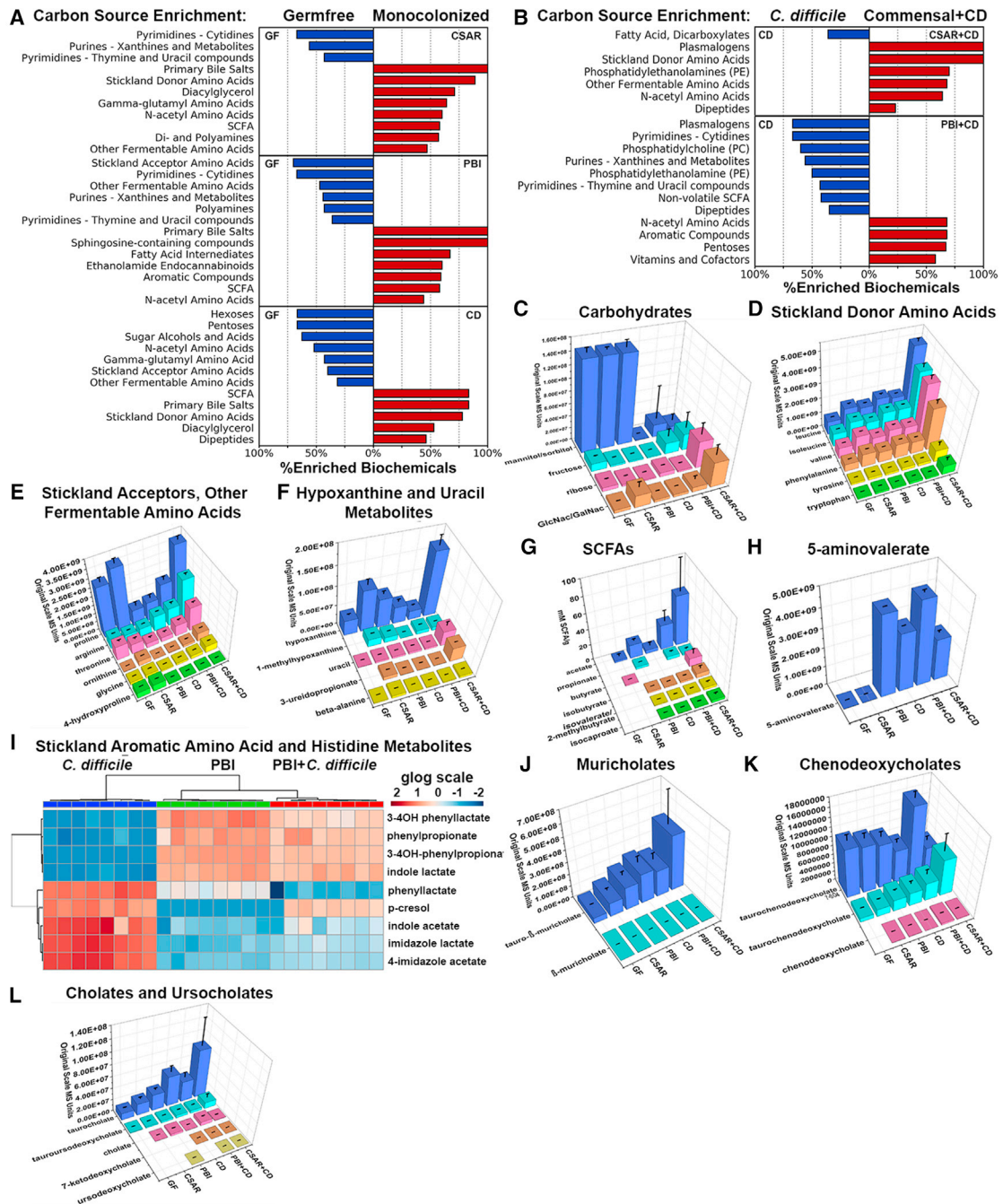


Figure 2. Commensal alteration of cecal carbon sources

(A) Significantly enriched carbon-source groups in germ-free (left) versus monocolonized mice (right), showing groups with a Benjamini-Hochberg corrected p value ≤ 0.05 . Horizontal bars indicate percentage of biochemicals enriched in each carbon-source group comparing germ-free cecal contents with *C. sardiniense*-monocolonized mice (CSAR) at 7 days (top); *P. bifementans* monocolonized mice (PBI) at 7 days (middle); or *C. difficile* monocolonized for 20 h (bottom).

(B) Significantly enriched carbon sources between *C. difficile* monocolonized mice at 20 h of infection (right) versus *C. sardiniense* monocolonized for 7 days + 20 h of *C. difficile* infection (top) or *P. bifementans* monocolonized for 7 days + 20 h of *C. difficile* infection (bottom). (C–H and J–L) Specifically enriched compounds (y axis) across colonization states (x axis). z axis shows original scale mass spectrometry counts. Error bars indicate standard deviation. Values for a given compound are comparable across experimental groups.

In panels (C)–(H), (J), and (K): stack-plot height indicates mean, error bars show standard error of the mean (SEM).

(C) Carbohydrates.

(D) Stickland donor amino acids.

(E) Stickland-acceptor and other fermentable amino acids.

(legend continued on next page)

depleted, including > 99% of mannitol and sorbitol and > 80% of fructose (Figure 2C).

C. difficile monocolonization produced acetate (Figure 2G) and Stickland branched-SCFA metabolites isobutyrate, isovalerate, 2-methylbutyrate, and isocaproate (Figure 2G). Aromatic amino acid metabolites specific to the pathogen's Stickland metabolism were also produced, including phenylacetate and phenyllactate from phenylalanine, indole acetate from tryptophan, and *p*-cresol from the *p*-hydroxyphenylacetate metabolite of tyrosine metabolism (Passmore et al., 2018; Steglich et al., 2018) (Figure 2I). *C. difficile* has a unique capacity to metabolize histidine-producing imidazole lactate and 4-imidazole acetate (Neumann-Schaal et al., 2019) (Figure 2I).

By 24 h of infection, with deteriorating mucosal conditions (Figures 1G and 1H), *C. sardiniense* and *C. difficile* co-colonized mice (Figure 2B, top) further enriched Stickland and other fermentable amino acids (Figures 2D and 2E), as gross blood, known to be abundant in Stickland-fermentable amino acids (Takach et al., 2014), entered the gut lumen (Figure 1H). Uracil levels increased > 8-fold and 3-ureidopropionate increased > 40-fold compared with *C. difficile* monocolonized mice (Figure 2F). In contrast, *P. bifermentans* and *C. difficile* co-colonized mice showed nominal differences in amine-containing carbon sources compared to *C. difficile* monocolonized mice (Figures 2D and 2E). *P. bifermentans*-specific aromatic amino acid metabolites predominated in the co-colonized state, with reduced levels of *C. difficile*-specific histidine metabolites, suggesting a dominance of *P. bifermentans*'s Stickland metabolism (Figure 2I). These findings illustrated *C. sardiniense*'s capacity to create a nutrient-enriched environment for *C. difficile* while *P. bifermentans* depleted preferred nutrients.

Microbial colonization altered additional host and microbial-origin metabolites. All three species enriched primary bile acids capable of inhibiting *C. difficile* germination, including β -muricholate (Figure 2J), and chenodeoxycholate (Figure 2L), and others with germination-stimulatory effects including cholate and taurocholate (Figure 2K) (Francis et al., 2013; Sorg and Sonenshein, 2009). All three species deconjugated host taruine-conjugated bile acids per detectable cholate, ursodeoxycholate (Figure 2L) and chenodeoxycholate (Figure 2K). In contrast, only *C. difficile* demonstrated 7α -hydroxysterol dehydrogenase activity (Bakonyi and Hummel, 2017) per detectable 7-ketodeoxycholate in mono- and co-colonized states (Figure 2L). *P. bifermentans* increased host-origin compounds with anti-inflammatory and neurotransmitter activities, including ethanolamide endocannabinoids, sphingosine-containing compounds, and metabolites of amino acid fermentations (Figure 2B, middle) (Lee et al., 2016).

P. bifermentans and *C. sardiniense* differentially modulate *C. difficile* gene expression in vivo

The commensal alterations in gut nutrients drove global perturbations in *C. difficile* gene expression (Figures 3A–3D). In monocolonized mice *C. difficile* induced transport and metabolic systems for glucose, fructose, ribose, and disaccharides (Figures 3A and 3C), dipeptides and oligopeptides, and Wood-Ljungdahl pathway genes for CO₂ fixation to acetate. By 24 h the pathogen upregulated ethanolamine utilization genes, enabling the capacity to use ethanolamine and amino-alcohol lipids from damaged mucosa (Nawrocki et al., 2018).

With *C. sardiniense*'s enrichment of amino acids and polyamines, *C. difficile* upregulated amino acid and polyamine transporters, pathways to convert *C. sardiniense*-enriched ornithine to Stickland-fermentable substrates (Fonknechten et al., 2009), and its Stickland proline reductase and reductive leucine-pathway genes (Figures 4A and 4B).

With *P. bifermentans* co-colonization (Figures 3C and 3D), *C. difficile* adapted its metabolism to available nutrients, upregulating genes to utilize sugar alcohols, particularly for mannitol and galactitol transport, followed by sorbitol, disaccharides, and polysaccharides—carbon sources not utilized by *P. bifermentans* (Moore, 1993). *C. difficile* also upregulated genes for the transport and metabolism of xanthines (Bradshaw, 1960) concomitant with *P. bifermentans*' enrichment of these compounds.

In the presence of either commensal, *C. difficile* downregulated cobalamin (Figures 3A–3D), and folate biosynthesis genes when co-colonized with *C. sardiniense* (Figure 3A), suggesting commensal-*C. difficile* cross-feeding with these nutrients.

Commensal colonization profoundly altered the pathogen's cellular machinery. With *C. sardiniense* co-colonization, *C. difficile* upregulated genes associated with transcription and DNA replication (Figures 3A and 3B). In contrast, by 20 h in *P. bifermentans* co-colonized mice, the pathogen significantly downregulated translation, ribosome production, and ATP synthesis (Figures 4C and 4D).

C. difficile-expressed stress-response genes as host inflammation evolved (Costa et al., 2016; Knippel et al., 2020), responses altered with commensal co-colonization. By 20 h of infection *C. difficile* monocolonized mice enriched CRISPR-gene expression and two temperate bacteriophage (Arndt et al., 2019) with homology to phiMMP01 (locus 3; Figure 3A), and phiCDHM19 (locus 2; Figure 3A). Diffocin-lytic genes (Gebhart et al., 2015), a phage-origin locus induced by quorum sensing, which can lyse other *C. difficile*, and cell-wall turnover enzymes were also enriched.

(F) Hypoxanthine and uracil metabolites.

(G) Cecal SCFAs. Z axis shows mM of SCFA per gram of cecal contents.

(H) Proline Stickland metabolite 5-aminovalerate.

(I) Heatmap of *C. difficile* and *P. bifermentans*-specific Stickland aromatic amino acid and histidine metabolites in cecal contents at 24 h of infection. Color scale shows generalized logarithm (log)-transformed mass spectroscopy metabolite counts. Hierarchical clustering by Pearson similarity and minimum-distance linkage are shown by metabolite on the left y axis.

(J–L) Specifically enriched compounds (y axis) across colonization states (x axis). z axis shows original scale mass spectrometry counts. Error bars indicate standard deviation. Values for a given compound are comparable across experimental groups.

(J) Muricholate.

(K) Chenodeoxycholate.

(L) Cholate and ursodeoxycholate bile acids among conditions.

Additional supporting information are found in Data S1 and S5.

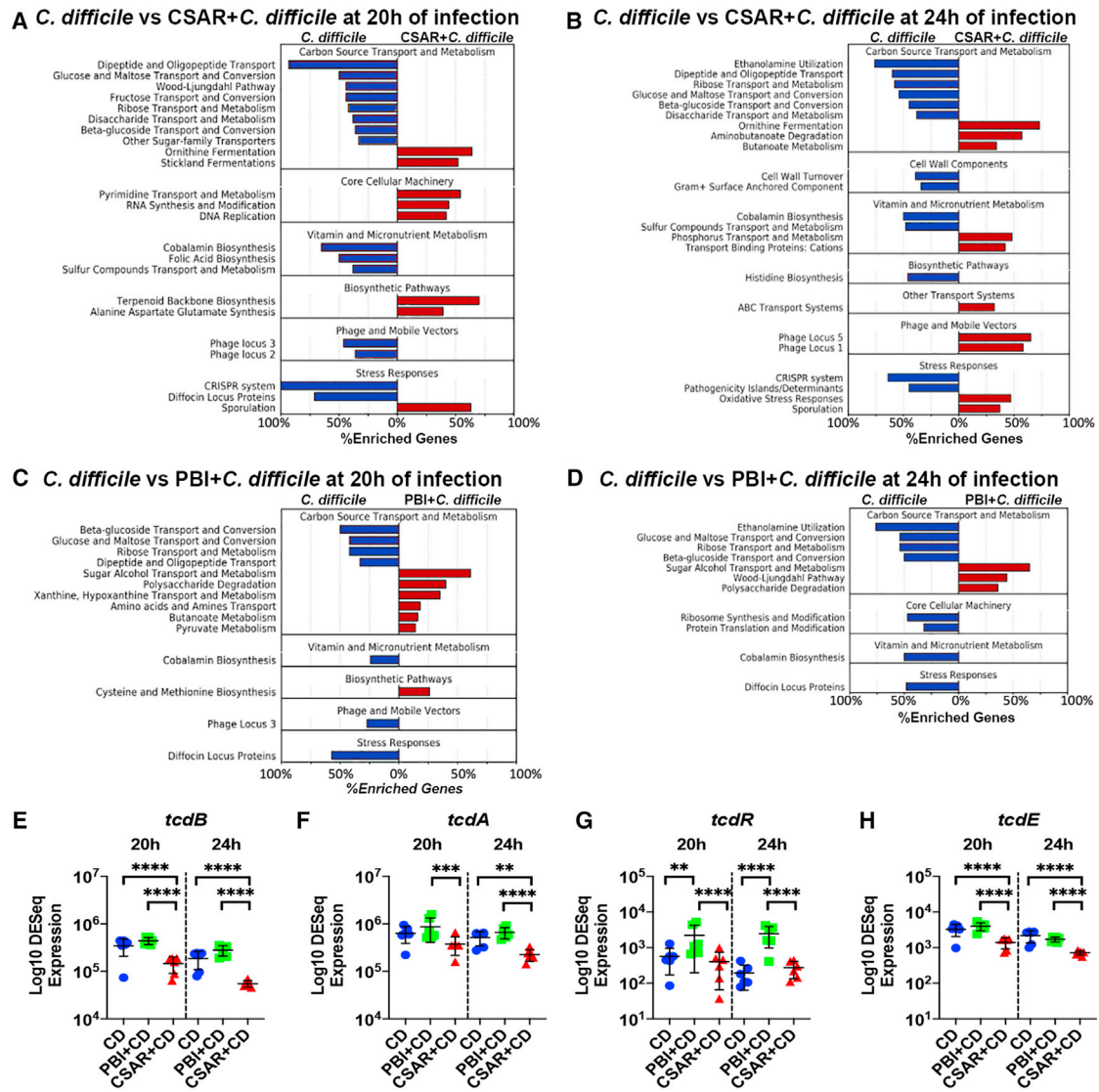


Figure 3. *C. difficile*-expressed pathways enriched in vivo

Horizontal bars indicate the percentage of genes enriched within the pathway in *C. difficile* monocolonized mice (left) or in mice co-colonized with *C. sardiniense* or *P. bifementans* prior to *C. difficile* infection (right). Pathways with a Benjamini-Hochberg adjusted p value ≤ 0.05 are shown.

(A) *C. difficile* monocolonized mice at 20 h of infection versus *C. sardiniense* and *C. difficile* co-colonized mice. (B) Comparison in panel (A) at 24 h of infection. (C) Comparison of *C. difficile* monocolonized with *P. Bifermentans* co-colonized mice at 20 h of infection. (D) Comparison in panel (C) at 24 h of infection.

(E–H) DESeq-normalized reads for the PaLoc genes: (E) *tcdA*, (F) *tcdB*, (G) *tcdR*, and (H) *tcdE*. X axis indicates the colonization condition; Y axis the \log_{10} DESeq read counts normalized for biomass differences. Bars show mean and standard deviation. Brackets indicate significant DESeq2 adjusted p values: * $0.01 < p \leq 0.05$; ** $0.001 < p \leq 0.01$; *** $0.0001 < p \leq 0.001$; **** $p \leq 0.0001$ Additional supporting information is found in [Data S2](#) and [Data S8](#).

In *C. sardiniense* co-colonized mice, *C. difficile* induced sporulation pathways and oxidative-stress responses, including nitroreductases, spore-associated superoxide dismutase (*sodA*), catalase (*cotG*), and genes for terpenoid backbone synthesis, peptidoglycan and spore-coat components with anti-oxidant activities (Bosak et al., 2008). Two additional bacteriophage loci with homology to phiMMP03 (loci 1 and 5; Figure 3B) were induced. In contrast, none of these systems showed upregulation with *P. bifementans* co-colonization (Figures 3C and 3D).

Each commensal differentially affected *C. difficile*'s PaLoc expression, which, in combination with alterations in pathogen

biomass, impacted toxin levels and host disease (Figures 1I and 1J). The biomass-adjusted expression of *tcdB*, *tcdA*, and *tcdE* in *C. difficile* monocolonized and *P. bifementans* co-colonized mice remained comparable at 20 and 24 h of infection (Figures 3E–3G), in spite of a 12-fold increase in *tcdR* expression in *P. Bifermentans* co-colonized mice (Figure 3H). While *C. sardiniense* co-colonized mice showed reduced *tcdB*, *tcdA*, and *tcdE* expression at 20 and 24 h of infection, these effects occurred in the context of higher pathogen vegetative biomass and released toxin in cecal contents (Figures 1I and 1J).

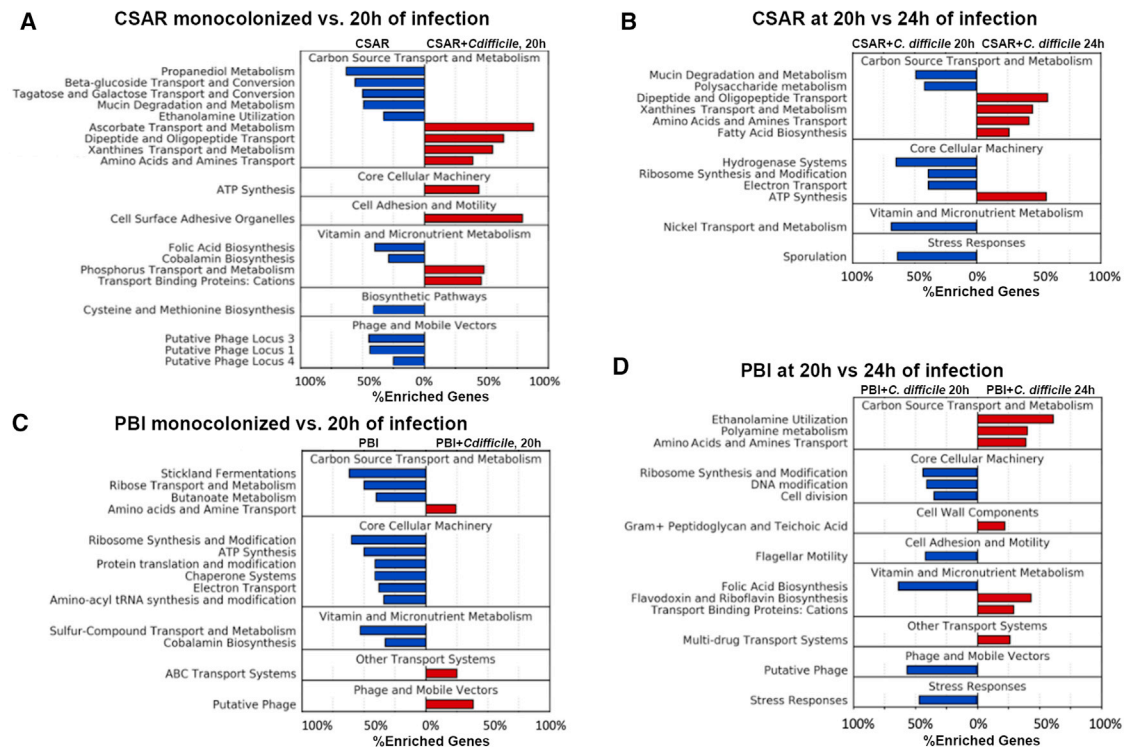


Figure 4. Commensal transcriptome analyses

Significantly enriched pathways in *C. sardiniense* and *P. bifermentans* monocolonized mice and with *C. difficile* infection. Pathways with Benjamini-Hochberg adjusted p values ≤ 0.05 are shown. The left-hand y axis shows enriched pathways; x axis indicates the percentage of enriched genes per category.

(A) *C. sardiniense*-monocolonized mice at 7 days prior to *C. difficile* infection versus after 20 h of *C. difficile* infection.

(B) *C. sardiniense* and *C. difficile* co-colonized mice at 20 versus 24 h of infection.

(C) *P. bifermentans* monocolonized mice at 7 days versus after 20 h of *C. difficile* infection.

(D) *P. bifermentans* and *C. difficile* co-colonized mice at 20 versus 24 h of infection. Additional supporting information is found in [Data S3](#), [S4](#), and [S8](#).

C. difficile infection profoundly alters commensal gene expression

C. difficile infection also systematically altered each commensal's gene expression, metabolism, and stress responses (Figures 4A–4D). *C. sardiniense*-monocolonized mice expressed systems involved in mucin degradation and metabolism and in the biosynthesis of cobalamin and folate (Figure 4A). Three bacteriophage loci, two with homology to *Clostridial* bacteriophage vB_CpeS_CP51 (loci 3 and 1), and one with homology to phiCT19406B (locus 4; Figure 4A, bottom), were also induced (Arndt et al., 2019).

By 20 h of infection, concomitant with evolving mucosal damage, *C. sardiniense* profoundly downregulated its mucin-degradation machinery (Figure 4A), while inducing genes for ascorbate transport and metabolism (Figure 4A)—systems that protect against oxidative stress. Multiple peptide and amino acid transport systems, and genes involved in the transport and metabolism of xanthines, were enriched. By 24 h *C. sardiniense* had profoundly downregulated ribosome production and sporulation. Energy generation and transport by 24 h of infection were also significantly affected with downregulation of multiple electron-transport systems and *C. sardiniense*'s nickel-based hydrogenase (Figure 4B) while upregulating the expression of F-type ATP-synthesis genes (Figure 4B).

In monocolonized mice, *P. bifermentans* showed high expression of its Stickland reductase systems (Figure 4C) in addition to protein translation and export and energy generation. As with *C. sardiniense*, *P. bifermentans* upregulated cobalamin synthesis genes. By 20 h of infection these processes showed reduced gene expression compared with the monocolonized state (Figure 4C) with enrichment of multiple amino acid transport systems and a putative bacteriophage with homology to phiCT19406A (Arndt et al., 2019). By 24 h of infection, *P. bifermentans* induced expression of genes for ethanolamine utilization (Figure 4D), suggesting a retooling of its metabolism for newly available carbon sources from damaged mucosa, in addition to genes for riboflavin transport and biosynthesis. Multiple stress-response systems, including *lexA*, *relA*, and CSP-family cold-shock proteins were downregulated by 24 h of infection, in addition to genes involved in ribosome production, cell division, and flagellar motility (Figure 4D).

Differential contributions of commensal arginine fermentation on C. difficile virulence

C. sardiniense and *P. bifermentans* can each ferment arginine to ornithine via the arginine deiminase (ADI) pathway, a system that *C. difficile* lacks (Pols et al., 2021). However, *C. difficile*, *P. bifermentans*, and other Stickland fermenters can convert

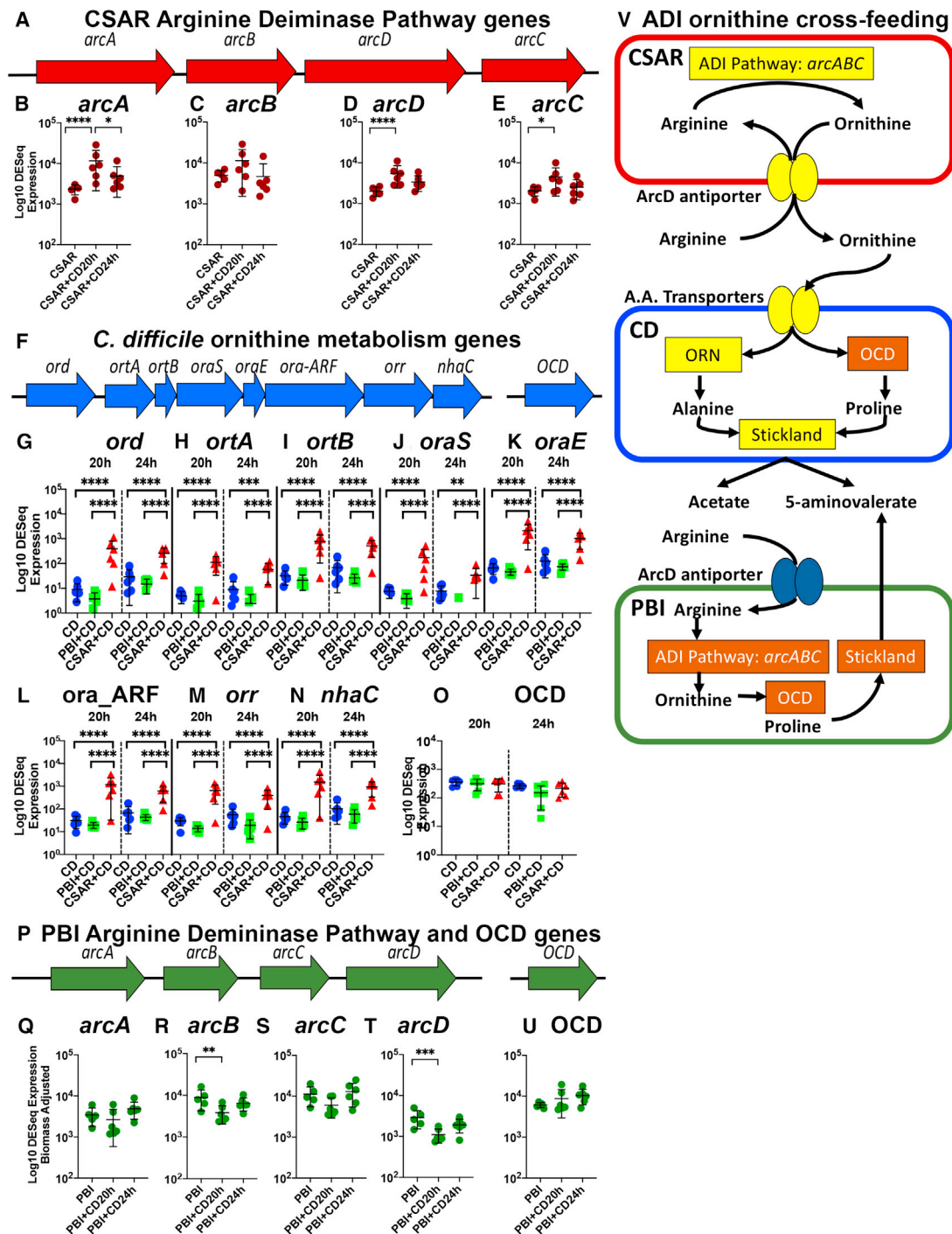


Figure 5. Commensal-pathogen ornithine cross-feeding

(A) *C. sardiniense*'s arginine deiminase pathway genes.

(B–E) \log_{10} DESeq2 normalized ADI gene expression. Bars show mean and standard deviation. (B) *arcA*, arginine deiminase (**** $p = 0.0001$; * $p = 0.0387$). (C) *arcB*, ornithine carbamoyltransferase. (D) *arcD*, arginine:ornithine antiporter (**** $p = 0.0008$). (E) *arcC*, carbamate kinase (* $p = 0.0259$).

(F) *C. difficile* ornithine to alanine conversion genes (operon_0246) and unlinked ornithine cyclodeaminase (UAB_RS0203800).

(G–O) DESeq2 normalized expression for operon_0246 genes. Bars show mean and standard deviation. Significance values indicated with * $0.01 \leq p < 0.05$; ** $0.001 \leq p < 0.01$; *** $0.0001 < p \leq 0.001$; **** $p \leq 0.0001$.

(G) *ord*, 2,4-diaminopentanoate dehydrogenase.

(H) *ortA*, 2-amino-4-ketopentanoate thiolase α subunit.

(I) *ortB*, β subunit.

(J) *oraS*, D-ornithine aminomutase S component.

(legend continued on next page)

ornithine to Stickland-fermentable substrates (Fonknechten et al., 2009). The species-level context of the ADI pathway demonstrated very different outcomes on *C. difficile* growth and host survival (Figure 5).

By 20 h of infection, *C. sardiniense* upregulated expression of its *arcA* arginine deiminase (Figure 5B), *arcC* carbamate kinase (Figure 2E), and *arcD* arginine-ornithine antiporter (Figure 2D), which imports arginine and exports the ornithine product, identifying a cause for the elevated ornithine in *C. sardiniense*-monocolonized mice (Figure 2E). In *C. difficile* the most strongly enriched genes with *C. sardiniense* co-colonization converted ornithine to alanine (Figures 5F–5N), a product able to support oxidative Stickland metabolism, cell-wall and protein synthesis, and other growth-promoting pathways (Peltier et al., 2011; Shrestha et al., 2017). *C. difficile*'s *OraSE* D-ornithine aminomutase (Figures 5J and 5K) requires cobalamin (Chen et al., 2001), another factor for which *C. sardiniense* induced biosynthetic gene expression prior to *C. difficile*'s introduction (Figure 4A). The pathogen's ornithine cyclodeaminase (Figure 5F), which converts ornithine to the Stickland-acceptor proline, remained constitutively expressed (Figure 5O).

In contrast to *C. sardiniense*, at 20 h of infection *P. bifementans* downregulated its *arcD* arginine-ornithine antiporter (Figures 5P and 5T) while maintaining constitutive expression of its ornithine cyclodeaminase (Figure 5U), thereby conserving a proline-convertible carbon source for its Stickland metabolism (Figure 5D).

Figure 5V illustrates putative interspecies effects of ADI fermentation on *C. difficile* *in vivo*. While the non-Stickland fermenter *C. sardiniense*-enriched luminal ornithine for *C. difficile*'s use, *P. bifementans*'s combined ADI and Stickland pathways supported its own metabolism and growth, depriving *C. difficile* of these growth-promoting carbon sources.

Systems biology models predict epistatic effects of *C. difficile*'s *CodY* and *CcpA* PaLoc metabolic repressors on pathogen phenotypes *in vivo*

CcpA and *CodY* repress *C. difficile* toxin expression when sufficient GTP, Stickland-fermentable substrates, and carbohydrates support metabolism (Dubois et al., 2016). Their absence supports toxin gene derepression. PRIME model predictions have inferred additional epistatic effects of *codY* and *ccpA* on the pathogen's ability to grow *in vivo* (Arrieta-Ortiz et al., 2021). Using recently optimized genetic manipulation systems to create serial deletion mutants in *C. difficile* (STAR Methods), we evaluated the effects of these regulators in the gnotobiotic and *P. Bifermentans* co-colonized states (Figure 6).

The *C. difficile* mutants $\Delta codY$, $\Delta ccpA$, and double $\Delta codY\Delta ccpA$ were each lethal in monocolonized mice while *P. bifementans* co-colonized mice survived (Figure 6A). Pathogen cecal biomass and toxin levels identified *P. bifementans*'s effects on toxin production among strains (Figures 6B–6D). *P. bifementans* co-colonized mice infected with the $\Delta ccpA$ mutant demonstrated reduced *C. difficile* vegetative biomass and toxin at 16 h (Figures 6B and 6C). At 24 h of infection, toxin levels were comparable between colonization states with the mutant and fell >80% after 14 days in surviving *P. Bifermentans* co-colonized mice (Figure 6C).

In contrast, $\Delta codY$ infected mice had better growth with *P. Bifermentans* co-colonization, while the double mutant grew poorly (Figure 6B). At 16 h of infection the $\Delta codY$ mutant showed comparable vegetative biomass in monocolonized and co-colonized states and elevated spore biomass in *P. Bifermentans* co-colonized mice (Figure 6D). Toxin levels with the $\Delta codY$ mutant were elevated at 16 h compared with wild-type controls, although levels in *P. Bifermentans* co-colonized mice were 70% lower than in $\Delta codY$ monocolonized controls (Figure 6C). However, from 16 to 24 h, toxin levels fell >40-fold in *P. Bifermentans* co-colonized mice (Figure 6D), in spite of the $\Delta codY$ mutant's higher vegetative biomass at 24 h in co-colonized mice (Figure 6B).

In *C. difficile* monocolonized mice PRIME model predictions inferred single- and double-mutant strain dysregulation of central carbon metabolism, as well as lipid and nucleotide biosynthesis, limiting growth in this nutrient-rich state as compared with wild type (Figure 6E) (Arrieta-Ortiz et al., 2021). In contrast, in the *P. bifementans* nutrient-depleted state (Figure 6F), PRIME predicted single *CodY* or *CcpA* deletion to be nonessential for mutant growth relative to wild type, but severe growth repression in the double mutant per epistatic interactions of *CodY* and *CcpA* on genes supporting metabolism of remaining gut-available carbon sources—namely sugar alcohols, polysaccharides, and supporting electron-transport systems—combined with dysregulation of essential genes in lipid, cell-wall, and nucleotide biosynthesis (Arrieta-Ortiz et al., 2021). These findings illustrated *P. bifementans*'s continued protection in the absence of the *CodY* and *CcpA* metabolic PaLoc repressors and predicted putative targets within these regulators that modulate the pathogen's adaptations to diverse *in vivo* environments.

P. bifementans bacteriotherapy rescues infected conventional mice

To assess *P. bifementans*'s use as a therapeutic, clindamycin-treated conventional mice were orally challenged with

(K) *oraE*, D-ornithine aminomutase E component.

(L) *ora_ARF*, reactivating factor for adenosylcobalamine-dependent D-ornithine aminomutase.

(M) *orr*, ornithine racemase.

(N) *nhaC*, Na⁺/H⁺ antiporter.

(O) Ornithine cyclodeaminase (OCD) expression.

(P) Schematic of *P. bifementans* ADI and OCD genes. Bars show mean and standard deviation.

(Q) *arcA*, arginine deiminase.

(R) *arcB*, ornithine carbamoyltransferase.

(S) *arcC*, carbamate kinase.

(T) *arcD*, arginine-ornithine antiporter (*p = 0.0227).

(U) OCD.

(V) Schematic showing differing effects of the ADI arginine fermentation in *C. sardiniense* and *P. bifementans* on *C. difficile* metabolism.

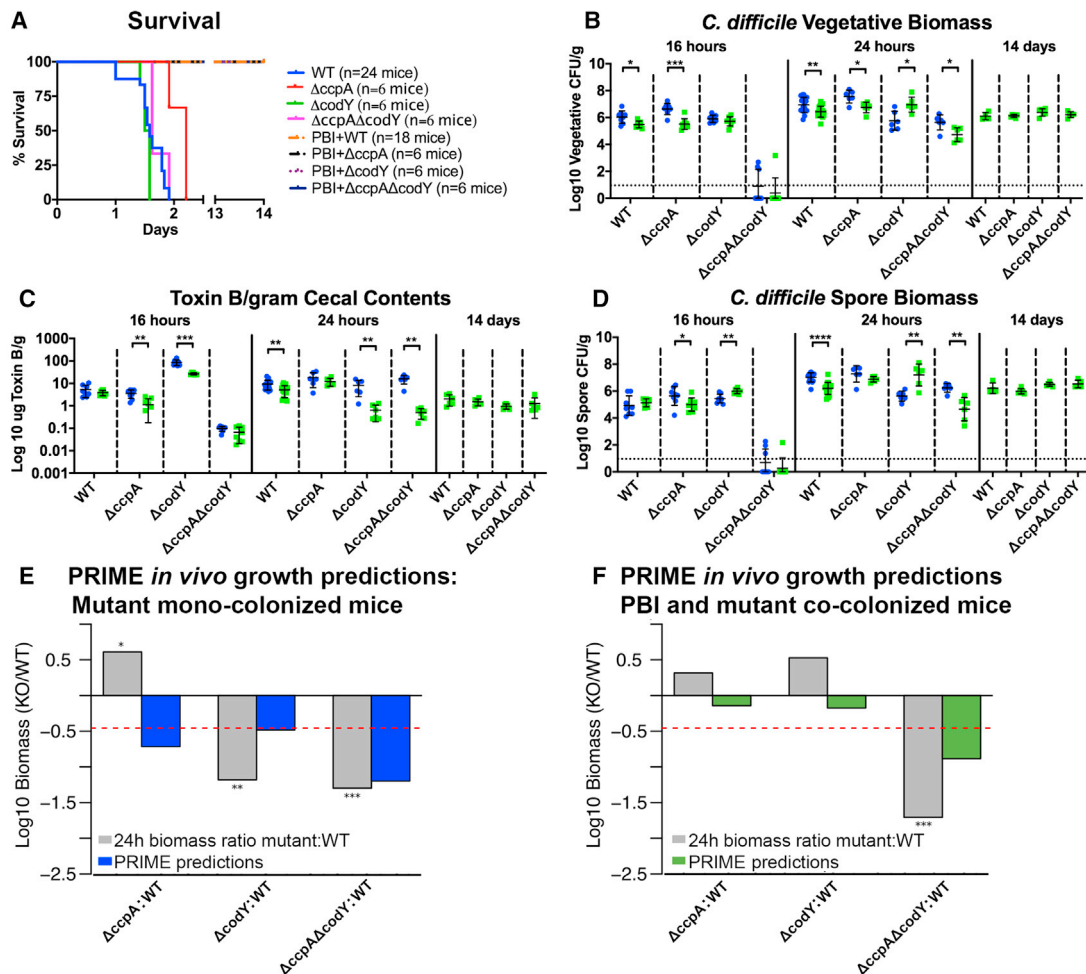


Figure 6. Combinatorial effects of *C. difficile*'s CodY and CcpA PaLoc metabolic repressors on infection in mono- and *P. bifementans* co-colonized mice

(A) Survival curves of GF and *P. bifementans* co-colonized mice infected with *C. difficile* wild-type (WT) or mutant strains ($n \geq 6$ mice per group). All *P. bifementans* co-colonized mice survived and differed significantly from monocolonized controls ($p < 0.0001$). $\Delta codY$ -infected mice declined more rapidly than WT infected mice ($p = 0.01$), while lethality in $\Delta ccpA$ -infected mice was delayed ($p = 0.0002$).

(B–D) Cecal biomass and extracellular toxinB levels. Bars show mean and standard deviation. *C. difficile*-associated mice (blue); mice monocolonized with *P. bifementans* and infected with *C. difficile* (green). Asterisks indicate Mann-Whitney p values: * $0.01 < p \leq 0.05$; ** $0.001 < p \leq 0.01$; *** $0.0001 < p \leq 0.001$; **** $p \leq 0.0001$.

(B) \log_{10} of μg toxinB levels per gram of cecal contents.

(C) Cecal \log_{10} of *C. difficile* vegetative cells (D) Spores at 16 h, 24 h, and 14 days in surviving *P. bifementans* co-colonized mice.

(E and F) Ratio of actual mutant to WT strain growth at 24 h of infection (gray bars) versus PRIME model predictions in monocolonized (blue bars) and *P. bifementans* co-colonized mice (green bars), respectively. Asterisks indicate significant t test p values in comparisons of mutant versus wild-type *C. difficile* strain growth at 24 h of infection; * < 0.05 , ** < 0.01 , *** < 0.001 . Dashed red lines indicate the PRIME threshold below which a given mutant is predicted to limit *in vivo* growth relative to WT. Additional supporting information of host body mass changes and *P. bifementans* biomass is found in Figure S2.

1,000 *C. difficile* spores. At the onset of symptomatic infection mice received 10^8 CFU of *P. bifementans* or vehicle-only control by gavage (Figure 7A). All *P. bifementans*-treated mice survived while control-treated mice demonstrated 40% lethality (Figure 7B, $p = 0.0061$). At 30 h after *C. difficile* challenge, at the height of symptomatic infection, *P. bifementans*-treated mice demonstrated reduced toxin levels and pathogen vegetative and spore biomass (Figures 7C–7E). By 14 days, surviving mice had low to undetectable toxin (Figure 7C) and had largely cleared both species (Figures 7D and 7E).

Clindamycin treatment enriched multiple carbon sources able to support *C. difficile* and *P. bifementans* growth including Stickland-acceptor amino acids, polyamines, and γ -glutamyl amino acids (Figures 7F and 7G), nutrients that were also enriched in *C. sardiniense*-monocolonized mice (Figure 2A). In control infected mice, the pathogen-depleted oligosaccharides, pentoses, and Stickland-acceptor and γ -glutamyl amino acids (Figure 7G, top). With *P. bifementans* treatment, these and additional compounds were depleted (Figure 7G, bottom). Clindamycin treatment also depleted host ethanolamine endocannabinoids and sphingosines, which showed improved recovery

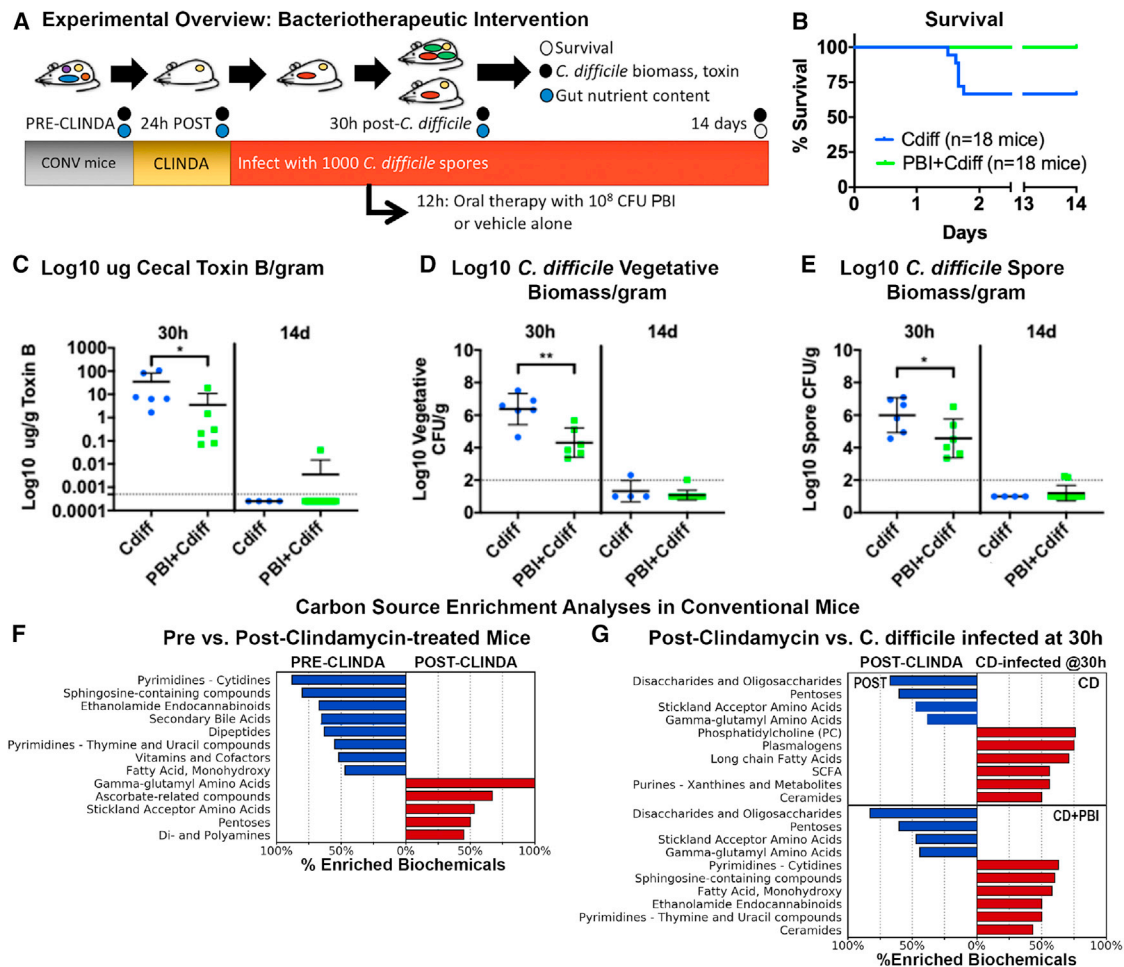


Figure 7. *P. bifementans* oral bacteriotherapy protects *C. difficile*-infected conventional mice

(A) Experimental overview. Samples for timed analyses (circles) were taken before and after clindamycin, at 30 h post-infection (12 h post-treatment), and at 14 days in surviving mice.

(B) Survival curve; blue: *C. difficile*-infected and vehicle control treated; green: *P. bifementans*-treated mice showed improved survival ($p = 0.0081$).

(C–E) Cecal toxin and *C. difficile* biomass. Bars show mean and standard deviation. Horizontal dotted line shows thresholds of detection. (C) Log₁₀ μg ToxinB/g in cecal contents ($p = 0.026$). (D) Cecal log₁₀ *C. difficile* vegetative (** $p = 0.0087$) and (E) spore biomass ($p = *0.0411$).

(F) Carbon-source enrichment analyses in mice pre and post-clindamycin treatment show enriched groups with a Benjamini-Hochberg corrected p value ≤ 0.05 .

(G) Enriched carbon source groups between post-clindamycin-treated and mice at 30 h of infection with *C. difficile* (top) or with *P. bifementans* treatment (bottom). Additional supporting information of host body mass changes and *P. bifementans* biomass are found in Figure S3. Supporting data for carbon-source enrichment results are found in Data S5 and S9.

in *P. bifementans*-treated mice (Figure 7G). These findings validated *P. bifementans*'s therapeutic efficacy in an infected conventional host through reductions in pathogen biomass and toxin.

DISCUSSION

We leveraged systems biology approaches to understand *C. difficile*'s *in vivo* responses to protective versus disease-promoting commensals. Using a tractable gnotobiotic infection model, we identified the remarkably protective effects of a single commensal species, *P. bifementans*, against *C. difficile*, and the capacity for another *Clostridial* species, *C. sardiniense*, to cause worse disease. Findings informed interventional studies in conventional, antibiotic-treated mice where *P. bifementans*

administration rescued infected mice from lethal infection. These findings have important implications to treat and prevent *C. difficile* infections, including that residual microbiota and those in uncharacterized FMT preparations can contain both protective and disease-exacerbating species that may exhibit different behaviors in antibiotic-depleted versus intact microbiota.

The development and severity of *C. difficile* infection occurs as a function of the pathogen's biomass, toxin production, and duration to which host tissues are exposed to the toxin. Each commensal modulated *C. difficile*'s virulence through multiple mechanisms (graphical abstract). Commensal colonization altered the gut-nutrient environment per enrichment or depletion of *C. difficile*-preferred carbon sources and required micronutrients, factors that modulated the pathogen's growth, stress responses, and toxin production.

Commensal colonization also affected pathways impacting *C. difficile*'s cellular integrity. *C. difficile* in monocolonized mice upregulated diffocins, a locus induced through quorum-sensing mechanisms that lyses a portion of the population, releasing toxin to promote mucosal damage and nutrient release to support surviving populations (Gebhart et al., 2015). Multiple temperate bacteriophage harboring lytic peptidoglycan hydrolases were induced in monocolonized and *C. sardiniense* co-colonized mice (Garneau et al., 2018). Sporulation also induces lytic transglycosylases, including UAB_RS0210585 (CD630_18980), a SigK-regulated gene believed to be involved in mother-cell lysis (Saujet et al., 2013), which was significantly upregulated in *C. difficile* and *C. sardiniense* co-colonized mice. While these processes have been demonstrated to contribute to toxin release in other toxigenic species, including *C. perfringens*, *Shigella*, and enterotoxigenic *E. coli* (ETEC) (Bielaszewska et al., 2012; Duncan, 1973; Meouche and Peltier, 2018), they warrant further analysis regarding their role in *C. difficile* pathogenesis.

In response to *C. sardiniense*'s enrichment of amine-containing carbon sources, *C. difficile* upregulated multiple amino acid transporters, Stickland fermentation pathways, and genes to convert *C. sardiniense*-enriched ornithine to Stickland-metabolizable substrates. *C. difficile* and *C. sardiniense* biomass expanded and, with nutrient release from damaged tissues, further stimulated microbial growth and toxin production, resulting in a rapidly lethal infection.

Notably, *C. sardiniense* and *P. bifermentans* possess arginine-deiminase fermentation pathways, a system that modulates very different effects *in vivo* with *C. difficile* infection (Figure 5E). With *C. sardiniense*, the commensal's export of ornithine provided one among many enriched nutrient sources for *C. difficile*. In contrast, *P. bifermentans*'s production of ornithine, with conversion to proline for its own metabolism, would deprive *C. difficile* of this nutrient source, while enhancing its ability to compete against the pathogen. This example highlights the importance of the underlying genomic and metabolomic context of pathways shared among commensal species when considering their effects on other microbes and on host phenotypes.

P. bifermentans limited *C. difficile*'s growth and toxin production through multiple mechanisms, including in the absence of *C. difficile*'s CodY and CcpA PaLoc repressors. As a glycolytic and active Stickland fermenter, *P. bifermentans* depleted fructose and amino acids preferred by *C. difficile*, leaving sugar alcohols, complex polysaccharides, and *P. bifermentans*-enriched hypoxanthines available. *C. difficile* adjusted its metabolism for these carbon sources but by 24 h of infection showed reduced biomass and toxin compared with monocolonized and *C. sardiniense* co-colonized mice. *P. bifermentans* co-colonization also downregulated pathogen genes supporting translation and ribosome production in addition to cellular lytic systems and oxidative stress pathways, suggesting additional mechanisms by which *P. bifermentans* could reduce the host's exposure to toxin (graphical abstract). PRIME model predictions inferred additional combinatorial effects of CodY and CcpA on gene networks for metabolic adaptations, electron transport, and biosynthetic reactions to support growth under the complex nutrient conditions encountered *in vivo*.

Host symptomatic infection, as evidenced by epithelial damage with neutrophil entry into the gut lumen, induced oxidative stress

systems in all three species. *C. difficile* and *C. sardiniense* strongly induced sporulation responses when co-colonized, including the spore-coat proteins superoxide dismutase (*sodA*) and manganese catalase (*cotG*), responses that may illustrate how sporulation in the confined space of the gut lumen can benefit vegetative cell populations of the same and other species by detoxifying host-produced ROS. Notably, *P. bifermentans* can grow in concentrations of up to 10% O₂ (STAR Methods) (Leja, 2014), conditions under which *C. sardiniense* and *C. difficile* cannot survive, an additional factor that may support its ability to compete with *C. difficile* during gut inflammation. *P. bifermentans* colonization also reduced the severity of the host's acute inflammatory responses (Figure 1E; graphical abstract), in part from reduced host exposure to high levels of *C. difficile* toxin (Figure 1I).

Interventional studies in antibiotic-treated conventional mice illustrated *P. bifermentans*'s efficacy as an oral bacteriotherapeutic. Clindamycin treatment enriched multiple amino acid and carbohydrate sources, including those enriched in GF and *C. sardiniense*-monocolonized mice, illustrating relevance of findings from germ-free infection studies to complex microbiota. These findings support a broader systems-level view for perturbations that create complex nutrient states conducive to *C. difficile* colonization and rapid growth *in vivo* given the pathogen's diverse carbon-source metabolism and adaptation to different gut environments. Notably, nutrient conditions enhancing *C. difficile* growth can also enhance the growth of commensal Stickland fermenters. Within the colon, unabsorbed dietary and host factors, mucins in particular, provide fermentable carbohydrates and amino acids, including the Stickland acceptors proline, glycine, and leucine (Wesley et al., 1985). However, disease-triggering antimicrobials to which *C. difficile* often harbors innate resistance, such as clindamycin, beta-lactams and fluoroquinolones, rapidly ablate competing Stickland fermenters, opening preferred nutrient sources for *C. difficile*'s rapid growth (Battaglioli et al., 2018; Peng et al., 2017) with risks for population crashes that can abruptly release toxin.

Stickland fermentation is a hallmark of cluster XI *Clostridial* metabolism and occurs in other *Clostridial* species, notably *Clostridium scindens* (cluster XIVa), which carries the proline and glycine reductases but lacks orthologous reductive leucine-pathway genes (STAR Methods). While conversion of progermination primary bile acids to germination-inhibitory secondary bile acids mediates aspects of *C. scindens*' protection against *C. difficile* (Buffie et al., 2015; Thanissery et al., 2017), we show capacity of commensals, singly or in aggregate, to rapidly change the gut-nutrient environment to modulate *C. difficile*'s virulence. Notably, the *P. bifermentans* and *C. sardiniense* strains used did not demonstrate 7 α -hydroxysterol-dehydrogenase activity in mice, while *C. difficile* did through its production of 7-ketodeoxycholate (Bakonyi and Hummel, 2017).

Stickland fermenters represent < 1% of the human gut microbiota. Our findings highlight the importance of these low-abundance species to consume *C. difficile* growth-promoting nutrients and identify complex conditions that other commensals, singly or in aggregate, could create to modulate *C. difficile*'s virulence. These conditions act in concert with the

host's digestive and immune functioning. Host and commensal effects may also explain why *C. difficile* phenotypes identified *in vitro* do not necessarily reflect behaviors seen *in vivo*. Armed with refined mechanistic knowledge, findings establish a robust framework in which to develop therapeutics with enhanced efficacy and improved safety for this disease.

STAR★METHODS

Detailed methods are provided in the online version of this paper and include the following:

- **KEY RESOURCES TABLE**
- **RESOURCE AVAILABILITY**
 - Lead contact
 - Materials availability
 - Data and code availability
- **EXPERIMENTAL MODEL AND SUBJECT DETAILS**
 - Bacterial strains and culture conditions
 - Construction of *C. difficile* mutant strains
 - Mouse studies
 - Gnotobiotic mouse colonization studies
 - Conventional mouse infection studies
- **METHOD DETAILS**
 - Histopathologic analyses
 - Toxin B ELISA
 - Effects of colonization on toxin function
 - Western blot for Toxin B integrity
 - Metabolomic studies
 - Cecal short chain fatty acid measurements
 - Carbon source enrichment analyses
 - Cluster analyses of Stickland metabolites
 - ATCC43255 and *C. sardiniense* genome annotation
 - *In vivo* bacterial RNA sequencing
 - Metatranscriptome data processing
 - Metatranscriptome enrichment analyses
 - Genomic DNA extraction and qPCR
 - *Clostridium scindens* Stickland reductase gene analysis
- **QUANTIFICATION AND STATISTICAL ANALYSIS**

SUPPLEMENTAL INFORMATION

Supplemental information can be found online at <https://doi.org/10.1016/j.chom.2021.09.007>.

ACKNOWLEDGMENTS

We thank Andrea Dubois, Cameron Friedman, Vladimir Yeliseyev, Qing Liu, Rebecca Krinzman, and Teri Bowman for technical support and Paul Sewell for graphic-design support. RNA sequencing was performed by the Harvard Medical School Biopolymers Core. Partners Healthcare's Eris team supported the Massachusetts Host-Microbiome Center's high performance computing resources. We also thank Jessica Allegretti, Laurent Bouillaut, Laurie Comstock, and Aimee Shen for critical reading of the manuscript and helpful comments. Funding: This work was supported by the BWH Precision Medicine Institute, R01AI153605 from the National Institute of Allergy and Infectious Diseases (NIAID) and P30DK034854 from the National Institute of Diabetes, Digestive and Kidney Diseases to L.B., R01AI128215, R01AI141953, and U19AI135976 from NIAID and IIBR-2042948 from the National Science Foundation to N.S.B.; B.P.G. was supported by T32 HL007627; the work of J.N.W. was supported by the Intramural Research Program of the National Library of

Medicine, National Institutes of Health. J.P. received support from the Institut Pasteur (Bourse ROUX). This work was conducted by authors from the FDA working as official U.S. Government employees and for which no additional external funding was utilized.

AUTHOR CONTRIBUTIONS

Conceptualization, L.B., A.L.S., and G.K.G.; methodology, B.P.G., N.D., J.N.W., J.P., M.L.A.-O., S.R.C.I., M.L.D., M.H., Y.L., N.G.-E., M.A., A.B.O., C.K.C., G.K.G., A.L.S., N.S.B., B.D., and L.B.; software, M.L.A.-O., S.R.C.I., N.S.B., J.N.W., and L.B.; formal analysis, B.P.G., N.D., J.N.W., M.L.A.-O., S.R.C.I., R.L., M.L.D., M.H., Y.L., N.G.-E., M.A., N.S.B., and L.B.; investigation, B.P.G., N.D., J.N.W., J.P., M.L.A.-O., S.R.C.I., R.L., M.L.D., A.L.S., N.S.B., B.D., and L.B.; resources, J.N.W., J.P., M.L.A.-O., S.R.C.I., M.L.D., M.H., Y.L., N.G.-E., M.A., A.B.O., B.D., A.L.S., N.S.B., and L.B.; data curation, J.N.W., M.L.A.-O., S.R.C.I., N.S.B., and L.B.; writing, L.B., N.D., B.P.G., J.N.W., J.P., M.L.D., M.H., and N.G.-E.; review and editing, B.P.G., N.D., J.N.W., M.L.A.-O., S.R.C.I., J.P., M.L.D., M.H., M.A., A.B.O., G.K.G., A.L.S., N.S.B., B.D., and L.B.; visualization, B.P.G., N.D., J.N.W., M.L.A.-O., S.R.C.I., N.S.B., and L.B.; supervision, L.B., B.D., N.S.B., and M.A.

DECLARATION OF INTERESTS

L.B. and G.K.G. are co-inventors on patents for *C. difficile* microbiota therapeutics. L.B., G.K.G., and A.L.S. are SAB members and hold stock in Pareto-Bio. G.K.G. is an SAB member and holds stock in Kaleido, Inc. A.L.S. is a co-owner of ExArca Pharmaceuticals. The remaining authors declare no competing interests.

Received: May 18, 2021

Revised: July 26, 2021

Accepted: September 16, 2021

Published: October 11, 2021

REFERENCES

- Abdel-Gadir, A., Stephen-Victor, E., Gerber, G.K., Noval Rivas, M., Wang, S., Harb, H., Wang, L., Li, N., Crestani, E., Spielman, S., et al. (2019). Microbiota therapy acts via a regulatory T cell MyD88/ROR γ t pathway to suppress food allergy. *Nat. Med.* **25**, 1164–1174.
- Allegretti, J.R., Marcus, J., Storm, M., Sitko, J., Kennedy, K., Gerber, G.K., and Bry, L. (2019). Clinical predictors of recurrence after primary Clostridioides difficile infection: a prospective cohort study. *Dig. Dis. Sci.* **65**, 1761–1766.
- Anders, S., Pyl, P.T., and Huber, W. (2015). HTSeq—a Python framework to work with high-throughput sequencing data. *Bioinformatics* **31**, 166–169.
- Andresen, J.R. (1994). Glycine metabolism in anaerobes. *Antonie Van Leeuwenhoek* **66**, 223–237.
- Arndt, D., Marcu, A., Liang, Y., and Wishart, D.S. (2019). PHAST, PHASTER and PHATEST: tools for finding prophage in bacterial genomes. *Brief. Bioinform.* **20**, 1560–1567.
- Arrieta-Ortiz, M.L., R., S., Turkarslan, S., Wu, W.J., Girinathan, B.P., Worley, J.N., DiBenedetto, N., Soutourina, O., Peltier, J., Dupuy, B., et al. (2021). Predictive regulatory and metabolic network models for systems analysis of Clostridioides difficile. *Cell Host Microbe* **29**. Published online October 11. <https://doi.org/10.1016/j.chom.2021.09.008>.
- Bakonyi, D., and Hummel, W. (2017). Cloning, expression, and biochemical characterization of a novel NADP $^{+}$ -dependent 7 α -hydroxysteroid dehydrogenase from Clostridium difficile and its application for the oxidation of bile acids. *Enzyme Microb. Technol.* **99**, 16–24.
- Baktash, A., Terveer, E.M., Zwittink, R.D., Hornung, B.V.H., Corver, J., Kuijper, E.J., and Smits, W.K. (2018). Mechanistic insights in the success of fecal microbiota transplants for the treatment of Clostridium difficile infections. *Front. Microbiol.* **9**, 1242.
- Nudel, K., Zhao, X., Basu, S., Dong, X., Hoffmann, M., Feldgarden, M., Allard, M., Klompas, M., and Bry, L. (2018). Genomics of Corynebacterium striatum, an emerging multidrug-resistant pathogen of immunocompromised patients. *Clin. Microbiol. Infect.* **24**, 1016.e7–1016.e13.

- Battaglioli, E.J., Hale, V.L., Chen, J., Jeraldo, P., Ruiz-Mojica, C., Schmidt, B.A., Rekdal, V.M., Till, L.M., Huq, L., Smits, S.A., et al. (2018). *Clostridioides difficile* uses amino acids associated with gut microbial dysbiosis in a subset of patients with diarrhea. *Sci. Transl. Med.* **10**, eaam7019.
- Beck, E.T., Buchan, B.W., Riebe, K.M., Alkins, B.R., Panchoi, P., Granato, P.A., and Ledebor, N.A. (2014). Multicenter evaluation of the Quidel Lyra Direct *C. difficile* nucleic acid amplification assay. *J. Clin. Microbiol.* **52**, 1998–2002.
- Belzer, C., Liu, Q., Carroll, M.C., and Bry, L. (2011). The role of specific IgG and complement in combating a primary mucosal infection of the gut epithelium. *Eur. J. Microbiol. Immunol. (Bp)* **1**, 311–318.
- Benjamini, Y.H., and Hochberg, Y. (1995). Controlling the false discovery rate: a practical and powerful approach to multiple testing. *J. R. Stat. Soc. B* **57**, 289–300.
- Berges, M., Michel, A.M., Lassek, C., Nuss, A.M., Beckstette, M., Dersch, P., Riedel, K., Sievers, S., Becher, D., Otto, A., et al. (2018). Iron regulation in *Clostridioides difficile*. *Front. Microbiol.* **9**, 3183.
- Bielaszewska, M., Idelevich, E.A., Zhang, W., Bauwens, A., Schaumburg, F., Mellmann, A., Peters, G., and Karch, H. (2012). Effects of antibiotics on Shiga toxin 2 production and bacteriophage induction by epidemic *Escherichia coli* O104:H4 strain. *Antimicrob. Agents Chemother.* **56**, 3277–3282.
- Bosak, T., Losick, R.M., and Pearson, A. (2008). A polycyclic terpenoid that alleviates oxidative stress. *Proc. Natl. Acad. Sci. USA* **105**, 6725–6729.
- Bouillaut, L., Dubois, T., Sonenshein, A.L., and Dupuy, B. (2015). Integration of metabolism and virulence in *Clostridium difficile*. *Res. Microbiol.* **166**, 375–383.
- Bouillaut, L., Self, W.T., and Sonenshein, A.L. (2013). Proline-dependent regulation of *Clostridium difficile* Stickland metabolism. *J. Bacteriol.* **195**, 844–854.
- Bradshaw, W.H., and Barker, H.A. (1960). Purification and properties of xanthine dehydrogenase from *Clostridium cylindrosporium*. *J. Biol. Chem.* **235**, 3620–3629.
- Bry, L., and Brenner, M.B. (2004). Critical role of T cell-dependent serum antibody, but not the gut-associated lymphoid tissue, for surviving acute mucosal infection with *Citrobacter rodentium*, an attaching and effacing pathogen. *J. Immunol.* **172**, 433–441.
- Bucci, V., Tzen, B., Li, N., Simmons, M., Tanoue, T., Bogart, E., Deng, L., Yeliseyev, V., Delaney, M.L., Liu, Q., et al. (2016). MDSINE: microbial Dynamical Systems INference Engine for microbiome time-series analyses. *Genome Biol* **17**, 121.
- Buffie, C.G., Bucci, V., Stein, R.R., McKenney, P.T., Ling, L., Gouberne, A., Liu, H., Kinnebrew, M., Viale, A., et al. (2015). Precision microbiome reconstitution restores bile acid mediated resistance to *Clostridium difficile*. *Nature* **517**, 205–208.
- Chen, H.P., Wu, S.H., Lin, Y.L., Chen, C.M., and Tsay, S.S. (2001). Cloning, sequencing, heterologous expression, purification, and characterization of adenosylcobalamin-dependent D-ornithine aminomutase from *Clostridium sticklandii*. *J. Biol. Chem.* **276**, 44744–44750.
- Chong, J., Soufan, O., Li, C., Caraus, I., Li, S., Bourque, G., Wishart, D.S., and Xia, J. (2018). MetaboAnalyst 4.0: towards more transparent and integrative metabolomics analysis. *Nucleic Acids Res* **46**, W486–W494.
- Costa, C.L., López-Ureña, D., de Oliveira Assis, T., Ribeiro, R.A., Silva, R.O., Rupnik, M., Wilcox, M.H., de Carvalho, A.F., do Carmo, A.O., Dias, A.A., et al. (2016). A MLST Clade 2 *Clostridium difficile* strain with a variant TcdB induces severe inflammatory and oxidative response associated with mucosal disruption. *Anaerobe* **40**, 76–84.
- Darling, A.E., Tritt, A., Eisen, J.A., and Facciotti, M.T. (2011). Mauve assembly metrics. *Bioinformatics* **27**, 2756–2757.
- Davis, J.J., Wattam, A.R., Aziz, R.K., Bretin, T., Butler, R., Butler, R.M., Chlenski, P., Conrad, N., Dickerman, A., Dietrich, E.M., et al. (2020). The PATRIC Bioinformatics Resource Center: expanding data and analysis capabilities. *Nucleic Acids Res* **48**, D606–D612.
- Dembek, M., Barquist, L., Boinett, C.J., Cain, A.K., Mayho, M., Lawley, T.D., Fairweather, N.F., and Fagan, R.P. (2015). High-throughput analysis of gene essentiality and sporulation in *Clostridium difficile*. *mBio* **6**, e02383.
- Dubois, T., Dancer-Thibonnier, M., Monot, M., Hamiot, A., Bouillaut, L., Soutourina, O., Martin-Verstraete, I., and Dupuy, B. (2016). Control of *Clostridium difficile* physiopathology in response to cysteine availability. *Infect. Immun.* **84**, 2389–2405.
- Duncan, C.L. (1973). Time of enterotoxin formation and release during sporulation of *Clostridium perfringens* type A. *J. Bacteriol.* **113**, 932–936.
- El Meouche, I., and Peltier, J. (2018). Toxin release mediated by the novel autolysin Cwp19 in *Clostridium difficile*. *Microb. Cell* **5**, 421–423.
- Fekete, S., Szakál, I., Andr ófszky, E., Kósa, E., and Hullár, I. (1996). Body composition of mice of different body condition score and sex. *Acta Vet. Hung.* **44**, 399–410.
- Fletcher, J.R., Erwin, S., Lanzas, C., and Theriot, C.M. (2018). Shifts in the gut metabolome and *Clostridium difficile* transcriptome throughout colonization and infection in a mouse model. *mSphere* **3**, e00089.
- Fonknechten, N., Perret, A., Perchat, N., Tricot, S., Lechaplais, C., Vallenet, D., Vergne, C., Zapparucha, A., Le Paslier, D., Weissenbach, J., and Salanoubat, M. (2009). A conserved gene cluster rules anaerobic oxidative degradation of L-ornithine. *J. Bacteriol.* **191**, 3162–3167.
- Francis, M.B., Allen, C.A., and Sorg, J.A. (2013). Muricholic acids inhibit *Clostridium difficile* spore germination and growth. *PLoS One* **8**, e73653.
- Gameau, J.R., Sekulovic, O., Dupuy, B., Soutourina, O., Monot, M., and Fortier, L.-C. (2018). High prevalence and genetic diversity of large phiCD211 (phiCDIF1296T)-like prophages in *Clostridioides difficile*. *Appl. Environ. Microbiol.* **84**, e02164.
- Gebhart, D., Lok, S., Clare, S., Tomas, M., Stares, M., Scholl, D., Donskey, C.J., Lawley, T.D., and Govoni, G.R. (2015). A modified R-type bacteriocin specifically targeting *Clostridium difficile* prevents colonization of mice without affecting gut microbiota diversity. *mBio* **6**, e02368.
- Girinathan, B.P., DiBenedetto, N., Worley, J., Peltier, J., Lavin, R., Delaney, M.L., Cummins, C., Onderdonk, A.B., Gerber, G.K., Dupuy, B., et al. (2020). The mechanisms of in vivo commensal control of *Clostridioides difficile* virulence. *bioRxiv*. <https://doi.org/10.1101/2020.01.04.894915>.
- Girinathan, B.P., Ou, J., Dupuy, B., and Govind, R. (2018). Pleiotropic roles of *Clostridium difficile* *sin* locus. *PLoS Pathog* **14**, e1006940.
- Griffith, O.W., Bridges, R.J., and Meister, A. (1979). Transport of gamma-glutamyl amino acids: role of glutathione and gamma-glutamyl transpeptidase. *Proc. Natl. Acad. Sci. USA* **76**, 6319–6322.
- Guo, Y., Li, C.-I., Ye, F., and Shyr, Y. (2013). Evaluation of read count based RNAseq analysis methods. *BMC Genomics* **14** (suppl 8), S2.
- Hofmann, J.D., Otto, A., Berges, M., Biedendieck, R., Michel, A.M., Becher, D., Jahn, D., and Neumann-Schaal, M. (2018). Metabolic reprogramming of *Clostridioides difficile* During the stationary phase With the induction of toxin production. *Front. Microbiol.* **9**, 1970.
- Huang, Y.Y., Martínez-Del Campo, A., and Balskus, E.P. (2018). Anaerobic 4-hydroxyproline utilization: discovery of a new glycol radical enzyme in the human gut microbiome uncovers a widespread microbial metabolic activity. *Gut Microbes* **9**, 437–451.
- Hunter, J.D. (2007). Matplotlib: a 2D graphics environment. *Comput. Sci. Eng.* **9**, 90–95.
- Jackson, S., Calos, M., Myers, A., and Self, W.T. (2006). Analysis of proline reduction in the nosocomial pathogen *Clostridium difficile*. *J. Bacteriol.* **188**, 8487–8495.
- Janoir, C., Denève, C., Bouttier, S., Barbut, F., Hoys, S., Caleechum, L., Chapetón-Montes, D., Pereira, F.C., Henriques, A.O., Collignon, A., et al. (2013). Adaptive strategies and pathogenesis of *Clostridium difficile* from in vivo transcriptomics. *Infect. Immun.* **81**, 3757–3769.
- Katarzyna Leja, K.M., Olkowicz, M., Juzwa, W., and Czaczyk, K. (2014). *Clostridium bifermentans* as an Aero-Tolerant Exponent of Strictly Anaerobe Genera. *Adv. Microbiol.* **4**, 216–224.
- Kim, J., Darley, D., Selmer, T., and Buckel, W. (2006). Characterization of (R)-2-hydroxyisocaproate dehydrogenase and a family III coenzyme A transferase

- involved in reduction of L-leucine to isocaproate by *Clostridium difficile*. *Appl. Environ. Microbiol.* **72**, 6062–6069.
- Kint, N., Janoir, C., Monot, M., Hoys, S., Soutourina, O., Dupuy, B., and Martin-Verstraete, I. (2017). The alternative sigma factor $\sigma(B)$ plays a crucial role in adaptive strategies of *Clostridium difficile* during gut infection. *Environ. Microbiol.* **19**, 1933–1958.
- Kirk, J.A., and Fagan, R.P. (2016). Heat shock increases conjugation efficiency in *Clostridium difficile*. *Anaerobe* **42**, 1–5.
- Knippel, R.J., Wexler, A.G., Miller, J.M., Beavers, W.N., Weiss, A., de Crécy-Lagard, V., Edmonds, K.A., Giedroc, D.P., and Skaar, E.P. (2020). *Clostridioides difficile* senses and hijacks host heme for incorporation into an oxidative stress defense system. *Cell Host Microbe* **28**, 411–421.e6.
- Kolmogorov, M., Yuan, J., Lin, Y., and Pevzner, P.A. (2019). Assembly of long, error-prone reads using repeat graphs. *Nat. Biotechnol.* **37**, 540–546.
- Langmead, B., and Salzberg, S.L. (2012). Fast gapped-read alignment with Bowtie 2. *Nat. Methods* **9**, 357–359.
- Lavin, R., DiBenedetto, N., Yeliseyev, V., Delaney, M., and Bry, L. (2018). Gnotobiotic and conventional mouse systems to support microbiota based studies. *Curr. Protoc. Immunol.* **121**, e48.
- Lee, Y., Jo, J., Chung, H.Y., Pothoulakis, C., and Im, E. (2016). Endocannabinoids in the gastrointestinal tract. *Am. J. Physiol. Gastrointest. Liver Physiol.* **311**, G655–G666.
- Leslie, J.L., Vendrov, K.C., Jenior, M.L., and Young, V.B. (2019). The gut microbiota is associated with clearance of *Clostridium difficile* infection independent of adaptive immunity. *mSphere* **4**, e00698.
- Mani, N., and Dupuy, B. (2001). Regulation of toxin synthesis in *Clostridium difficile* by an alternative RNA polymerase sigma factor. *Proc. Natl. Acad. Sci. USA* **98**, 5844–5849.
- Marcella, C., Cui, B., Kelly, C.R., Ianiro, G., Cammarota, G., and Zhang, F. (2021). Systematic review: the global incidence of faecal microbiota transplantation-related adverse events from 2000 to 2020. *Aliment. Pharmacol. Ther.* **53**, 33–42.
- Marco-Ramell, A., Palau-Rodríguez, M., Alay, A., Tulipani, S., Urpi-Sarda, M., Sanchez-Pla, A., and Andres-Lacueva, C. (2018). Evaluation and comparison of bioinformatic tools for the enrichment analysis of metabolomics data. *BMC Bioinformatics* **19**, 1.
- Martin-Verstraete, I., Peltier, J., and Dupuy, B. (2016). The regulatory networks that control *Clostridium difficile* toxin synthesis. *Toxins (Basel)* **8**, 153.
- Mead, G.C. (1971). The amino acid-fermenting clostridia. *J. Gen. Microbiol.* **67**, 47–56.
- Mills, J.P., Rao, K., and Young, V.B. (2018). Probiotics for prevention of *Clostridium difficile* infection. *Curr. Opin. Gastroenterol.* **34**, 3–10.
- Moore, L., and Moore, W.E.C. (1993). *Anaerobe Lab Manual*, Fourth Edition (VPI).
- Nawrocki, K.L., Wetzell, D., Jones, J.B., Woods, E.C., and McBride, S.M. (2018). Ethanolamine is a valuable nutrient source that impacts *Clostridium difficile* pathogenesis. *Environ. Microbiol.* **20**, 1419–1435.
- Neumann-Schaal, M., Hofmann, J.D., Will, S.E., and Schomburg, D. (2015). Time-resolved amino acid uptake of *Clostridium difficile* 630 Δ erm and concomitant fermentation product and toxin formation. *BMC Microbiol.* **15**, 281.
- Neumann-Schaal, M., Jahn, D., and Schmidt-Hohagen, K. (2019). Metabolism the *difficile* way: the key to the success of the pathogen *Clostridioides difficile*. *Front. Microbiol.* **10**, 219.
- Neumann-Schaal, M., Metzendorf, N.G., Troitzsch, D., Nuss, A.M., Hofmann, J.D., Beckstette, M., Dersch, P., Otto, A., and Sievers, S. (2018). Tracking gene expression and oxidative damage of O₂-stressed *Clostridioides difficile* by a multi-omics approach. *Anaerobe* **53**, 94–107.
- Neves, A.L.A., Li, F., Ghoshal, B., McAllister, T., and Guan, L.L. (2017). Enhancing the resolution of rumen microbial classification from metatranscriptomic data using Kraken and Mothur. *Front. Microbiol.* **8**, 2445.
- Passmore, I.J., Letertre, M.P.M., Preston, M.D., Bianconi, I., Harrison, M.A., Nasher, F., Kaur, H., Hong, H.A., Baines, S.D., Cutting, S.M., et al. (2018). Para-cresol production by *Clostridium difficile* affects microbial diversity and membrane integrity of Gram-negative bacteria. *PLoS Pathog* **14**, e1007191.
- Peltier, J., Courtin, P., El Meouche, I., Lemée, L., Chapot-Chartier, M.-P., and Pons, J.-L. (2011). *Clostridium difficile* has an original peptidoglycan structure with a high level of N-acetylglucosamine deacetylation and mainly 3–3 cross-links. *J. Biol. Chem.* **286**, 29053–29062.
- Peng, Z., Jin, D., Kim, H.B., Stratton, C.W., Wu, B., Tang, Y.-W., and Sun, X. (2017). Update on antimicrobial resistance in *Clostridium difficile*: resistance mechanisms and antimicrobial susceptibility testing. *J. Clin. Microbiol.* **55**, 1998–2008.
- Pettit, L.J., Browne, H.P., Yu, L., Smits, W.K., Fagan, R.P., Barquist, L., Martin, M.J., Goulding, D., Duncan, S.H., Flint, H.J., et al. (2014). Functional genomics reveals that *Clostridium difficile* Spo0A coordinates sporulation, virulence and metabolism. *BMC Genomics* **15**, 160.
- Pols, T., Singh, S., Deelman-Driessen, C., Gaastra, B.F., and Poolman, B. (2021). Enzymology of the pathway for ATP production by arginine breakdown. *FEBS Journal* **288**, 293–309.
- Pruss, K.M., and Sonnenburg, J.L. (2021). *C. difficile* exploits a host metabolite produced during toxin-mediated disease. *Nature* **593**, 261–265.
- Reeves, A.E., Koenigsnecht, M.J., Bergin, I.L., and Young, V.B. (2012). Suppression of *Clostridium difficile* in the gastrointestinal tracts of germ-free mice inoculated with a murine isolate from the family Lachnospiraceae. *Infect. Immun.* **80**, 3786–3794.
- Riley, M. (1993). Functions of the gene products of *Escherichia coli*. *Microbiol. Rev.* **57**, 862–952.
- Ryals, J., Lawton, K., Stevens, D., and Milburn, M. (2007). *Metabolon, Inc. Pharmacogenomics* **8**, 863–866.
- Saujet, L., Pereira, F.C., Serrano, M., Soutourina, O., Monot, M., Shelyakin, P.V., Gelfand, M.S., Dupuy, B., Henriques, A.O., and Martin-Verstraete, I. (2013). Genome-wide analysis of cell type-specific gene transcription during spore formation in *Clostridium difficile*. *PLoS Genet* **9**, e1003756.
- Sayers, E.W., Beck, J., Brister, J.R., Bolton, E.E., Canese, K., Comeau, D.C., Funk, K., Ketter, A., Kim, S., Kimchi, A., et al. (2020). Database resources of the National Center for Biotechnology Information. *Nucleic Acids Res* **48**, D9–D16.
- Schloss, P.D. (2020). Reintroducing mothur: 10 years later. *Appl. Environ. Microbiol.* **86**, e02343.
- Seemann, T. (2014). Prokka: rapid prokaryotic genome annotation. *Bioinformatics* **30**, 2068–2069.
- Shrestha, R., Lockless, S.W., and Sorg, J.A. (2017). A *Clostridium difficile* alanine racemase affects spore germination and accommodates serine as a substrate. *J. Biol. Chem.* **292**, 10735–10742.
- Sorg, J.A., and Sonenshein, A.L. (2009). Chenodeoxycholate is an inhibitor of *Clostridium difficile* spore germination. *J. Bacteriol.* **191**, 1115–1117.
- Steglich, M., Hofmann, J.D., Helmecke, J., Sikorski, J., Spröer, C., Riedel, T., Bunk, B., Overmann, J., Neumann-Schaal, M., and Nübel, U. (2018). Convergent loss of ABC transporter genes from *Clostridioides difficile* genomes is associated with impaired tyrosine uptake and p-cresol production. *Front. Microbiol.* **9**, 901.
- Takach, E., O’Shea, T., and Liu, H. (2014). High-throughput quantitation of amino acids in rat and mouse biological matrices using stable isotope labeling and UPLC-MS/MS analysis. *J. Chromatogr. B Analyt. Technol. Biomed. Life Sci.* **964**, 180–190.
- Thanissery, R., Winston, J.A., and Theriot, C.M. (2017). Inhibition of spore germination, growth, and toxin activity of clinically relevant *C. difficile* strains by gut microbiota derived secondary bile acids. *Anaerobe* **45**, 86–100.
- Theriot, C.M., Koenigsnecht, M.J., Carlson, P.E., Jr., Hatton, G.E., Nelson, A.M., Li, B., Huffnagle, G.B., Li, J.Z., and Young, V.B. (2014). Antibiotic-induced shifts in the mouse gut microbiome and metabolome increase susceptibility to *Clostridium difficile* infection. *Nat. Commun.* **5**, 3114.

- Valdés-Varela, L., Alonso-Guervos, M., García-Suárez, O., Gueimonde, M., and Ruas-Madiedo, P. (2016). Screening of bifidobacteria and lactobacilli able to antagonize the cytotoxic effect of *Clostridium difficile* upon intestinal epithelial HT29 monolayer. *Front. Microbiol.* **7**, 577.
- van den Berg, R.A., Hoefsloot, H.C., Westerhuis, J.A., Smilde, A.K., and van der Werf, M.J. (2006). Centering, scaling, and transformations: improving the biological information content of metabolomics data. *BMC Genomics* **7**, 142.
- Vogels, G.D., and Van der Drift, C. (1976). Degradation of purines and pyrimidines by microorganisms. *Bacteriol. Rev.* **40**, 403–468.
- Wattam, A.R., Davis, J.J., Assaf, R., Boisvert, S., Brettin, T., Bun, C., Conrad, N., Dietrich, E.M., Disz, T., Gabbard, J.L., et al. (2017). Improvements to PATRIC, the all-bacterial Bioinformatics Database and Analysis Resource Center. *Nucleic Acids Res* **45**, D535–D542.
- Wesley, A., Mantle, M., Man, D., Qureshi, R., Forstner, G., and Forstner, J. (1985). Neutral and acidic species of human intestinal mucin. Evidence for different core peptides. *J. Biol. Chem.* **260**, 7955–7959.
- Wick, R.R., Judd, L.M., Gorrie, C.L., and Holt, K.E. (2017). Unicycler: resolving bacterial genome assemblies from short and long sequencing reads. *PLoS Comput. Biol.* **13**, e1005595.
- Wilson, K.H., Sheagren, J.N., Freter, R., Weatherbee, L., and Lyerly, D. (1986). Gnotobiotic models for study of the microbial ecology of *Clostridium difficile* and *Escherichia coli*. *J. Infect. Dis.* **153**, 547–551.
- Worley, J., Delaney, M.L., Cummins, C.K., DuBois, A., Klompas, M., and Bry, L. (2020). Genomic determination of relative risks for *Clostridioides difficile* infection from asymptomatic carriage in ICU patients. *Clin. Infect. Dis.* <https://doi.org/10.1093/cid/ciaa894>.
- Zarandi, E.R., Mansouri, S., Nakhaee, N., Sarafzadeh, F., and Moradi, M. (2017). Toxin production of *Clostridium difficile* in sub-MIC of vancomycin and clindamycin alone and in combination with ceftazidime. *Microb. Pathog.* **107**, 249–253.
- Zheng, W., Wang, K., Sun, Y., and Kuo, S.-M. (2018). Dietary or supplemental fermentable fiber intake reduces the presence of *Clostridium XI* in mouse intestinal microbiota: the importance of higher fecal bacterial load and density. *PLoS One* **13**, e0205055.

STAR★METHODS

KEY RESOURCES TABLE

REAGENT or RESOURCE	SOURCE	IDENTIFIER
Antibodies		
toxin B ELISA - monoclonal antibody	BBI solutions, Madison, WI, USA	BM347-T4G1
toxin B ELISA - monoclonal antibody	BBI solutions, Madison, WI, USA	BM347-N4A8
Bacterial and virus strains		
<i>Clostridioides difficile</i>	ATCC, 10801 University Boulevard, Manassas, VA 20110, USA	ATCC 43255
<i>Clostridium sardiniense</i>	DSMZ, Inhoffenstraße 7B 38124 Braunschweig, Germany	DSM 599
<i>Paraclostridium bifermentans</i>	DSMZ, Inhoffenstraße 7B 38124 Braunschweig, Germany	DSM 14991
Chemicals, peptides, and recombinant proteins		
Streptavidin-HRP	Thermo-Fisher, Waltham, MA, USA	N504
Clindamycin phosphate	Millipore-Sigma, St. Louis, MO	PHR1021
<i>C. difficile</i> cell culture toxin assay	Quidel, San Diego, CA 92121, USA	03-05000
Polyscreen PVDF membrane	Perkin Elmer, Waltham, MA, 02451, USA	NEF1002
SuperSignal West Pico Plus Western Blotting Substrate	Thermo-Fisher, Waltham, MA, 02451, USA	34577
Ethyl ether	Millipore-Sigma, St. Louis, MO	EX0190-8
Boron trifluoride-methanol	Millipore-Sigma, St. Louis, MO	15716
Minion sequencing cartridge	Oxford Nanopore	MIN106D
Zymo Direct-zol RNA purification kit	Zymo, Irvine, CA	R2081
Ribo-Zero Gold rRNA removal kit	Illumina, San Diego, CA	MRZH116
NEBNext bacterial RNA kit	New England Biolabs, Ipswich, MA	E7850X
rRNA Depletion Kit	New England Biolabs, Ipswich, MA	E6310X
TruSeq mRNA Library Prep kit	Illumina, San Diego, CA	20020594, 20020493
NEBNext Ultra II Directional RNA library prep kit	New England Biolabs, Ipswich, MA	E7760L
Qubit dsDNA HS Assay Kit	Thermo-Fisher, Waltham, MA	Q32854
Zymo Quick-DNA Fecal/Soil Microbe Miniprep Kit	Zymo, Irvine, CA	11-322
PBS	Millipore-Sigma, St. Louis, MA	P3813-10PAK
Z-FIX	Thermo-Fisher, Waltham, MA	NC9351419
CHROMID® <i>C. difficile</i>	Biomérieux, Durham, NA	CHROMID® <i>C. difficile</i>
Brucella agar with 5% sheep's blood, hemin and vitK1	Becton Dickinson, Canaan, CT	8807311
BHI broth	Anaerobe Systems, Morgan Hill, CA	AS-872
Critical commercial assays		
Global Metabolomics	Metabolon, Raleigh, NC	Global Metabolomics Screen
RNA sequencing	HMS Biopolymers Core, Boston, MA	NextSeq sequencing services
Deposited data		
RNAseq data and CSAR genomic data	NCBI Bioproject https://www.ncbi.nlm.nih.gov/bioproject/	BioprojectID: PRJNA755661
<i>C. difficile</i> ATCC43255 closed genome	NCBI https://www.ncbi.nlm.nih.gov/genome/?term=NZ_CP049958.1	AccessionID: NZ_CP049958.1
Experimental models: Organisms/strains		
Swiss Webster Gnotobiotic Mice	Massachusetts Host-Microbiome Center	SWGf
Swiss Webster Conventional Mice	Taconic Farms, Taconic, NY	SW

(Continued on next page)

Continued

REAGENT or RESOURCE	SOURCE	IDENTIFIER
Oligonucleotides		
Table S1 oligonucleotides	IDT DNA http://www.idtdna.com/	Ordered direct from vendor
Recombinant DNA		
pMSR0	http://www.addgene.org/	78750
Software and algorithms		
Bowtie2	http://bowtie-bio.sourceforge.net/bowtie2/index.shtml	Bowtie 2.2.2
HTseq	https://pypi.org/project/HTSeq/	HTseq 0.11.1
Kraken2	https://ccb.jhu.edu/software/kraken2/	Kraken2
DESeq2	https://bioconductor.org/packages/release/bioc/html/DESeq2.html	DESeq2 1.26
Prism	GraphPad, San Diego, CA	Prism 8.0
Metaboanalyst	https://www.metaboanalyst.ca/	Metaboanalyst 4.0
Python	http://www.python.org/	Python 3.7.6
Matplotlib python library	https://matplotlib.org/	Matplotlib 3.4.2
OriginLab	http://www.originlab.com/	OriginLab 2021
MinKNOW	Oxford Nanopore	MinKNOW v3.6.5
Unicycler	https://github.com/rwrick/Unicycler	Unicycler v.0.4.8
Flye assembler	https://github.com/fenderglass/Flye	Flye 2.4.1
Mauve	http://darlinglab.org/mauve/mauve.html	Mauve 2.4.0
NCBI Prokaryotic Genome Automatic Annotation Pipeline	https://www.ncbi.nlm.nih.gov/genome/annotation_prok/	NCBI PGAP
PATRIC	https://www.patricbrc.org/	Genome Annotation Service
PROKKA	https://github.com/tseemann/prokka	PROKKA 1.13.7
PHASTER	https://phaster.ca	PHASTER bacteriophage annotation service

RESOURCE AVAILABILITY**Lead contact**

Lynn Bry, MD, PhD, lbry@bwh.harvard.edu

Materials availability

- Type collection strains are available from the ATCC (<http://www.atcc.org/>) and DSMZ strain collections (<http://www.dsmz.de>).
- The pMSR0 plasmid vector used for mutant construction has been deposited into Addgene, ID: 78750.
- Mutant strains in *C. difficile* ATCC43255 may be requested from Dr. Dupuy or Bry's laboratories or through the Crimson core resource (<https://crimson-core.partners.org/>). Users requesting infectious *C. difficile* isolates must provide institutional documentation for strain handling at biohazard level 2.
- Chemical reagents and supplies are available as per referenced vendors in the [STAR Methods](#).
- Gnotobiotic and conventional Swiss-Webster mice are available from Taconic Farms (Taconic, NY) or through the Massachusetts Host-Microbiome Center's gnotobiotic resource.

Data and code availability

- The updated *C. difficile* ATCC43255 reference genome has been deposited to NCBI under accession# NZ_CP049958.1.
- The *C. sardiniense* genome has been deposited to NCBI under accession# JAIKTU000000000.
- Metatranscriptomic datasets are available through NCBI under GEO ID: GSE182613.
- Carbon source maps, metabolomic datasets, and statistical results from metabolomic enrichment analyses are available in the supplemental Excel files GF_CarbonSourceEnrichment.xlsx and CONV_CarbonSourceEnrichment.xlsx.
- Microbial gene-level content and statistical results from metatranscriptomic analyses are available in the supplemental Excel files TranscriptomeGeneContent.xlsx and RNAseq_TranscriptomeEnrichment.xlsx.
- The open source python libraries and code for RNAseq analyses are available from the respective referenced sites in the [STAR Methods](#).

EXPERIMENTAL MODEL AND SUBJECT DETAILS

Bacterial strains and culture conditions

Table S1: Strains and Culture Conditions, Related to **STAR Methods** section: **Bacterial strains and culture conditions**, shows the bacterial strains and in vitro culture conditions. For quantitation of *C. difficile* and commensal biomass, mouse cecal contents were collected into pre-weighed Eppendorf tubes with 0.5mL of pre-reduced PBS with 40mM cysteine (Millipore-Sigma, St. Louis, MO) as a reducing agent. Tubes were weighed after adding material and transferred into a Coy anaerobic chamber (Coy Labs, Grass Lake, MI) at 37°C for serial dilutions with plating to selective *C. difficile* CHROMID® agar (Biomérieux, Durham, NC) or Brucella agar (Becton Dickinson, Canaan, CT) for commensal quantitation. *C. difficile* colonies were counted at 48 hours of incubation and identified as large black colonies. For the $\Delta\text{codY } \Delta\text{ccpA}$ double mutant, colonies were quantitated at 72 hours of incubation. Commensal colonies were counted after 24h of incubation. *C. sardiniense* were identified as small, round beta-hemolytic colonies, and *P. bifermentans* as opaque and larger round colonies. Representative colonies were species-confirmed by rapid ANA (Remel, Lenexa, KS). For studies in conventional mice, pre-infection and post-clindamycin fecal pellets showed no positive colonies on *C. difficile* CHROMID® agar.

For studies of microaerophilic growth, *P. bifermentans* was cultured in tryptone-yeast (TY) media with resazurin (Moore, 1993), without additional cysteine or other reducing agents, and that had been equilibrated to O₂ levels of 0.5%, 1%, 5% and 10% (n=3 cultures per condition). TY media exposed to 0.5% O₂ or higher levels of oxygen caused oxidation of the resazurin dye. Control samples were incubated in TY under anaerobic gas mix or ambient air (21% O₂) as a negative control. Samples were serially diluted and plated to Brucella agar after 24h of culture at 37°C to quantitate viable CFU.

C. difficile spore preparations and counts were defined by exposing pre-weighed material to 50% ethanol for 60 minutes followed by serial dilution and plating to *C. difficile* CHROMID® agar, as described (Bucci et al., 2016). Vegetative cell biomass was calculated by subtracting the spore biomass from the total biomass and normalizing to the cecal mass. Data were evaluated in Prism 8.0 (GraphPad, San Diego, CA) for visualization and log-rank tests of significance among groups. A p value <0.05 was considered significant.

Construction of *C. difficile* mutant strains

Table S2: Plasmids and Oligonucleotides Used, Related to **STAR Methods** section **Construction of *C. difficile* mutant strains**, indicates plasmid vectors and primer sequences (IDTDNA, Redwood City, CA) used to generate gene-deleted mutants in ATCC43255. Mutants were created using the toxin-mediated Allele-Coupled Exchange (ACE) vector (Girinathan et al., 2020). For deletions, allelic exchange cassettes were designed to have approximately 900 bp of homology to the chromosomal sequence in both up- and downstream locations of the sequence to be altered. The homology arms were amplified by PCR from *C. difficile* strain ATCC43255 genomic DNA and purified PCR products were cloned into the PmeI site of pMSR0 using NEBuilder's HiFi DNA Assembly. pMSR0-derived plasmids were transformed into *E. coli* strain NEB10β and inserts verified by sequencing. Plasmids were then transformed into *E. coli* HB101 (RP4) and transferred by conjugation into *C. difficile* ATCC43255 after a brief period of heat shock as described (Kirk and Fagan, 2016).

Mouse studies

All animal studies were conducted under an approved institutional IACUC protocol. Defined-colonization experiments were conducted in negative pressure BL-2 gnotobiotic isolators (Class Biologically Clean, Madison, WI). Conventional studies were conducted in OptiMice containment cages (Animal Care Systems, Centennial, CO) (Lavin et al., 2018). Mice were singly housed for all studies.

Gnotobiotic mouse colonization studies

One week prior to infection with *C. difficile* equal ratios of 6-7 week old male and female gnotobiotic mice were gavaged with 1x10⁸ CFU of *P. bifermentans*, *C. sardiniense*, or sterile vehicle control, and allowed to colonize for 7 days prior to challenge with 1x10³ of wild-type or mutant *C. difficile* spores. Fecal pellets from mice were cultured prior to infection to confirm association with the defined species, or maintenance of the GF state. Progression of disease was assessed via body condition scoring (Fekete et al., 1996) and body mass measurements taken by ethylene-oxide sterilized, battery powered OHAUS scales (Thermo-Fisher, Waltham, MA). Mice were sacrificed at a BCS of 2-, or at defined timepoints at 7 days of commensal monocolonization or GF controls, and at 20, 24h or 14 days post-*C. difficile* challenge. For *C. difficile* mutant infection studies, timepoints at 16h and 24h post-challenge were collected. Cecal contents were collected for functional studies. The GI tract and internal organs were fixed in zinc-buffered formalin (Z-FIX, Thermo-Fisher, Waltham, MA) for histopathologic assessment.

Conventional mouse infection studies

5-week old conventional mice (Taconic Farms, Inc., Taconic, NY) were singly housed and acclimated for a week prior to treatment with USP-grade clindamycin phosphate (10mg/kg; Sigma Chemical, St. Louis, MO) via intraperitoneal (IP) injection. 24 hours post-clindamycin treatment, mice were challenged with 1x10³ wild-type *C. difficile* spores via oral gavage and treated with 1x10⁸ CFU of *P. bifermentans* or vehicle control at 12h post *C. difficile* challenge, the earliest point of symptomatic diarrhea in conventional mice. Progression of disease was assessed via BCS and body mass measurements. Survival studies were followed to 14 days post *C. difficile* challenge. For *C. difficile* biomass, toxin B levels and cecal metabolomic studies, 12 mice per group were also sacrificed.

and cecal contents collected at pre-clindamycin treatment, post-clindamycin treatment just prior to *C. difficile* challenge, 30 hours post *C. difficile* challenge (18 hours after receiving *P. bifermentans* or vehicle control by gavage), and at 14 days following control or *P. bifermentans* treatment.

METHOD DETAILS

Histopathologic analyses

Formalin-fixed gut segments from GF or specifically-associated mice were paraffin embedded and 5 μ m sections cut for staining with hematoxylin and eosin (H&E; Thermo-Fisher, Waltham, MA) as described (Bry and Brenner, 2004). Slides were visualized under a Nikon Eclipse E600 microscope (Nikon, Melville, NY) to assess epithelial damage per cellular stranding and vacuolation, the nature of inflammatory infiltrates, mucosal erosions, and tissue edema. Luminal neutrophils were quantified by a Pathologist by evaluating ten 400X high powered fields (HPFs) across at least 3 colonic sections per mouse. Neutrophils were identified by presence of segmented nuclei and pale to finely granular cytoplasm (Belzer et al., 2011). Data were plotted in Prism and comparisons among colonization states by timepoint evaluated by Mann-Whitney log-rank test.

Toxin B ELISA

Cecal toxin B levels were quantified as described (Zarandi et al., 2017). Briefly, microtiter plates were coated with 5 μ g/mL of anti-TcdB capture antibody (BBI solutions, Madison, WI). Supernatants of spun cecal contents and standard curve controls of toxin B (ListLabs, Campbell, CA) were assayed in triplicate. After incubation and washing with anti-toxin B biotinylated antibody (mouse-anti-*C. difficile* TcdB; BBI solutions, Madison, WI) followed by high Sensitivity Streptavidin-HRP conjugate (Thermo-Fisher, Waltham, MA), signal was detected with TMB substrate (Thermo-Fisher, Waltham, MA) at 450nm using a BioTek Synergy H1 plate reader (Biotek Instruments Inc, Winooski, VT). Values were analyzed in Prism 8.0 (GraphPad, San Diego, CA) to calculate μ g of toxin B/gram of cecal contents. Significant differences among groups were evaluated by non-parametric Kruskal-Wallis ANOVA and Dunn's post-test. A p value ≤ 0.05 was considered significant.

Effects of colonization on toxin function

The Quidel *C. difficile* cell culture functional toxin assay (Beck et al., 2014) was used to evaluate if commensal colonization altered the functional toxicity of *C. difficile* toxin. Cecal contents were collected from germfree mice or from mice monocolonized for 7 days with *P. bifermentans*, or *C. sardiniense*. 100 μ L of purified toxin B control solution (Quidel Inc., San Diego, CA) was added to 1 gram of cecal contents and incubated for 30 minutes prior to making 1:10 to 1:500 serial dilutions in the Quidel-provided dilution buffer and adding materials to confluent cultures of human MRC-5 fibroblasts. Fibroblast cells were incubated at 37 $^{\circ}$ C for 48 hours and checked daily by compound microscope for signs of cytopathic effect (CPE) indicated by balling up of cells and loss of adhesion. Additional control samples included cecal contents incubated with toxin B for 30 minutes followed by addition of neutralizing antibody to confirm specificity of CPE by toxin B. Cells where CPE occurred in the presence of toxin B, but not with cecal contents alone or with neutralizing antibody were called positive. All conditions were repeated in triplicate. The highest dilution at which CPE occurred was identified for each condition.

Western blot for Toxin B integrity

Cecal supernatants from mice at 20h of infection were subjected to SDS-PAGE and transferred to PVDF membrane (PerkinElmer, Waltham, MA) as described (Girinathan et al., 2018). Toxin B was detected by using Sheep Primary Antibody, Donkey Secondary Antibody (R&D Systems, Minneapolis MN), diluted 1:1000 in 5% nonfat dry milk blotting buffer (25mM Tris, pH 7.4, 0.15M NaCl, 0.1% Tween 20), and by chemiluminescence using the SuperSignal West Pico Plus Western Blotting Substrate (part# 34577; Thermo-Scientific, Waltham, MA).

Metabolomic studies

For GF colonization studies cecal contents from 8 mice per group across 2 experimental replicates were harvested from GF mice at baseline, after 7 days of monocolonization with *P. bifermentans* or *C. sardiniense*, and at 24h post-infection with *C. difficile* alone or with each commensal (6 groups, 48 mice total). For conventional studies, cecal contents were collected from 12 mice per group prior to clindamycin treatment, 24h post-clindamycin treatment prior to *C. difficile* challenge, and at 30h post *C. difficile* challenge, at the height of symptomatic infection. Materials were snap frozen into pre-weighed tubes and weighed to determine mass of cecal contents. Global metabolomic screen of samples was performed by Metabolon (Raleigh, NC) with sample extraction and MALDI-TOF analyses as described (Fletcher et al., 2018; Ryals et al., 2007). Results were obtained as Original Scale mass spectrometry counts.

Cecal short chain fatty acid measurements

Volatile short chain fatty acids from specifically-associated mice (n=6 mice/group across two experimental replicates) were quantified as described (Moore, 1993). In brief, acidified internal standards with 100 μ L of ethyl ether anhydrous or boron trifluoride-methanol was added to 100 μ L of supernatant from homogenized cecal contents. Chromatographic analyses were carried out on an Agilent 7890B system with flame ionization detector (FID). Chromatogram and data integration were carried out using the OpenLab ChemStation software (Agilent Technologies, Santa Clara, CA). SCFA in samples were identified by comparing their specific retention times relative to the retention time in the standard mix. Concentrations were determined and expressed as mM of each SCFA per gram of sample for

the raw cecal/fecal material. The Agilent platform cannot discriminate the isomers isovalerate and 2-methylbutyrate and thus reports these compounds out as a single peak and interpolated value.

Carbon source enrichment analyses

A variation of pathway enrichment analysis (Marco-Ramell et al., 2018) was used to evaluate carbon source availability and consumption *in vivo*. Curated carbon source groups, optimized to reflect carbon source metabolism of gut commensal species, were developed with review of primarily literature regarding anaerobic metabolism of carbohydrate, amino acid and other amine-containing compounds, lipids, aromatic compounds, purines and pyrimidines, vitamins, micronutrients and other input sources for microbial metabolism and growth. Additional sources of reviewed information included published maps of *C. difficile*'s biochemical pathways (Janoir et al., 2013; Pettit et al., 2014) and BioCyc and MetaCyc content for *C. difficile* strain CD630 (Marco-Ramell et al., 2018). A carbon source group required a minimum of 6 biochemicals for evaluation. For studies in GF mice, 506 biochemicals, of 787 identified by the Metabolon panel, 64.3% of the dataset, were curated into carbon source groups. For studies in conventional mice, 667 biochemicals of 858, 77.8% of the dataset, were curated into carbon source groups. The carbon source mappings and results in specifically-associated and conventional mice are available in supplemental files [Data S6: Carbon Source Enrichment Analyses in Specifically-associated Mice, Related to Figure 2](#) and [STAR Methods](#) section: [Carbon source enrichment analyses](#), and [Data S9: Carbon Source Enrichment Analyses in Conventional Mice, Related to Figure 7](#) and [STAR Methods](#) section: [Carbon source enrichment analyses](#).

Mass spectrometry datasets were filtered to remove biochemicals with values <50,000 counts across all samples (<3% of biochemicals). Remaining zero-value data points were assigned a value of 25,000 to support calculation of Log₂ fold-change between comparisons. Datasets were Log₂ transformed for significance testing of each biochemical by Welch's T test and Benjamini-Hochberg multi-hypothesis correction (Benjamini, 1995; van den Berg et al., 2006). Thresholds for enrichment used a Log₂ fold-change of ≥0.32192809 (1.25X), and a Log₂ fold-change ≤ -0.32192809 (-1.25X) for depletion, and per-biochemical adjusted p value ≤0.05. Biochemicals in pairwise comparisons were ranked by adjusted p value and up to the top 40% of significantly changing biochemicals were used in analyses.

The number of enriched and depleted biochemicals per carbon source group, and total number of enriched and depleted biochemicals in datasets were calculated. Carbon source groups with ≥4 enriched or ≥4 depleted biochemicals underwent hypothesis testing by hypergeometric test, followed by Benjamini-Hochberg multi-hypothesis correction (Benjamini, 1995). An adjusted p value ≤0.05 for enriched or depleted carbon source groups was considered significant. Significantly enriched or depleted groups were plotted using the Python library Matplotlib (Hunter, 2007). Results for biochemicals within enriched groups were plotted in OriginLab (Origin Lab, Wellesley Hills, MA) using the 3D XYY function, or with the Metaboanalyst 4.0 visualization tools (Chong et al., 2018).

Cluster analyses of Stickland metabolites

Stickland aromatic amino acid and histidine metabolites with known specificity for *C. difficile* or *P. bifementans* (Mead, 1971; Neumann-Schaal et al., 2019) were clustered by mouse sample using the Metaboanalyst 4.0 clustering tools and Pearson's correlation matrices (Chong et al., 2018). Similarities among samples were evaluated by *omova* (Schloss, 2020).

ATCC43255 and *C. sardiniense* genome annotation

Given discrepancies for multiple genes and bacteriophage loci in the RefSeq genome for *C. difficile* ATCC43255, a closed, reference genome was generated using Oxford Nanopore Gridlon sequencing (Oxford Nanopore Technologies, Oxford, UK) according to the manufacturer's instructions. The prepared library was sequenced on a MIN106D flow cell (R9.4.1) for 72 hours using the fast calling model. Reads were base called in real-time and demultiplexed using MinKNOW v3.6.5. The genome was *de novo* assembled using reads >5 kb in size with Flye v2.4.1 (Kolmogorov et al., 2019) to produce one circular contig with 400X coverage and size of 4,313,281 bp. A second hybrid assembly using the nanopore long reads with short reads generated by Miseq sequencing (GenBank: SRS5656519) was generated using Unicycler v.0.4.8 (Wick et al., 2017). Mauve (Darling et al., 2011) was used to align and determine the synteny of both assemblies.

To correct potential stop codon and frameshift sequencing errors in coding regions, the hybrid assembly was compared to 26 pre-existing *de novo* SPAdes assemblies for ATCC43255 generated using Illumina MiSeq data from Worley, et al. (Worley et al., 2020). The corrected genomic data is available in NCBI under Accession#: NZ_CP049958.1.

The updated reference genome was annotated using the NCBI Prokaryotic Genome Automatic Annotation Pipeline (Sayers et al., 2020), PATRIC (Wattam et al., 2017), and PROKKA (Seemann, 2014) to extract gene features for support of transcriptome pathway enrichment analyses. Bacteriophage loci and genes were identified using PHASTER (Arndt et al., 2019).

A genome for *C. sardiniense* (GenBank: SRR15509127) was generated using the methods of a in Nudel, et al. by Illumina MiSeq and annotated as described (Nudel et al., 2018). To assess presence of a putative ornithine cyclodeaminase gene, the *C. sardiniense* genome was subjected to nucleotide and protein BLAST using the ornithine cyclodeaminase nucleotide coding regions and amino acid sequences from *C. difficile* ATCC43255 (geneID: UAB_RS0202485), *P. bifementans* (geneID: fig|1490.7.peg.2150), the cluster I *Clostridium*, *Clostridium botulinum* (GenBank: WP_072587252), and *Enterococcus faecalis* (GenBank: WP_002358614.1). No orthologous genes in *C. sardiniense* were identified.

In vivo bacterial RNA sequencing

RNA was extracted from 15–20mg of flash frozen cecal contents (n=6 mice per group) using the Zymo Direct-zol RNA purification kit (R2081; Zymo, Irvine, CA). The quality of extracted RNA was assessed using an Agilent 2100 Bioanalyzer (Agilent Technologies, Lexington, MA) and samples with RNA Integrity Number (RIN) \geq 8.0 were processed through Ribo-Zero Gold rRNA removal kit (MRZH116; Illumina, San Diego, CA) or NEBNext bacterial and rRNA Depletion Kit to deplete prokaryotic and eukaryotic rRNAs, and eukaryotic poly-A mRNAs (New England Biolabs, Ipswich, MA). The transcriptome sequencing libraries were constructed using the Illumina TruSeq mRNA Library Prep kit (20020594, 20020493; Illumina, San Diego, CA) or NEBNext Ultra II Directional RNA library prep kit (New England Biochemical, Ipswich, MA), per the manufacturer's specifications. Library sizes were checked using a Bioanalyzer DNA High Sensitivity chip and TapeStation and quantified using Qubit dsDNA HS Assay Kit (Q32854; Thermo-Fisher, Waltham, MA). For sequencing runs, 12 libraries were pooled and sequenced on an Illumina Nextseq500 (Illumina, San Diego, CA) in paired-end 150 (PE150) nucleotide runs.

Metatranscriptome data processing

To map reads to gene features, the *P. bifementans* ATCC638 (DSM14991) reference genome, NZ_AVNC01000001.1, was obtained from PATRIC (Davis et al., 2020) and *Mus musculus* C57BL6/J genome, GCF_000001635.26, from NCBI. The genomes for *C. difficile* ATCC43255 and *C. sardiniense* DSM599 were generated as described. The annotated gene content used in analyses for all three species is in supplemental file [Data S7: Metatranscriptome Gene Content, Related to STAR Methods sections Metatranscriptome Data Processing, and Metatranscriptome Enrichment Analyses](#).

Paired-end reads were quality filtered and trimmed then mapped to mouse and microbial genomes using Bowtie2 (Langmead, 2012) using strict requirements for read orientation. The “–no-mixed” and “–no-discordant” flags were used to ensure that paired reads aligned to the same section of the genome in the expected orientation, respectively. Read pairs with a mapping quality <10 , a measure of alignment uniqueness, were filtered. Reads aligning to >1 genome was flagged for subsequent analysis to identify potential sites of homology among genomes.

Mapped reads were assigned to gene features using HTSeq (Anders et al., 2015) with flags “–nonunique all” to allow reads mapping to multiple features to be called to account for polycistronic RNAs, and “–a 10” to set the minimum mapping quality score at 10, a measure of alignment uniqueness. The identity of unaligned reads was analyzed with Kraken2 (Neves et al., 2017) to confirm association of mice with the expected species.

HTSeq results from each experimental replicate were binned by species and formatted for DESeq2 analyses (Guo et al., 2013). Gene features where no set of experimental replicates averaged more than 10 reads per replicate were filtered from further analysis ($<3\%$ of genes). A widely used DESeq2 analysis template was modified for differential expression analysis (<https://gist.github.com/stephenturner/f60c1934405c127f09a6>). Read data from all experimental replicates of a given organism were included for pairwise DESeq2 analyses to ensure the same adjusted read counts and estimates of dispersion across pairwise comparisons.

Metatranscriptome enrichment analyses

For *C. difficile*, mappings leveraged multiple previously published gene-level and pathway annotations for CD630 (Dembek et al., 2015; Hofmann et al., 2018; Janoir et al., 2013), assignments of gene function in the *C. difficile* EGRIN model (Arrieta-Ortiz et al., 2021), and the bacterial-based Riley schema (Riley, 1993) to define microbial pathways and super-pathways, with addition of pathways such as “Mucin Degradation” to describe commensal-host categories, or ones that were missing or incompletely annotated in public resources. An operon map of *C. difficile* genes was created from the BioCyc content for CD630 (Marco-Ramell et al., 2018). Genes present in ATCC43255, but not CD630, were treated as single-cistron operons. PATRIC and PROKKA (Seemann, 2014) annotation of the *C. sardiniense* and *P. bifementans* genomes were used to develop pathway maps for these species. Gene features in the commensals were also subjected to BLAST against the CD630 reference genome to provide additional annotation information. The annotated microbial gene features are shown in supplemental file [Data S7: Metatranscriptome Gene Content, Related to STAR Methods sections: Metatranscriptome Data Processing, and Metatranscriptome Enrichment Analyses](#).

A minimum of 8 genes across at least 2 putative operon structures were required to define a pathway category. Thresholds for gene enrichment or depletion were set at $\pm 1.5X$ fold-change (Log_2 fold-change of ± 0.584962501) and with a DESeq2 per-gene adjusted p value ≤ 0.05 . Up to the top 40% of significantly changing genes, ranked by the per-gene adjusted p value, were analyzed in each pairwise comparison. Pathways with a minimum of 5 enriched or of 5 depleted genes underwent hypothesis testing by hypergeometric test. Multi-hypothesis adjusted p values were calculated using the Benjamini-Hochberg method (Benjamini, 1995). Pathways with an adjusted p value ≤ 0.05 were considered significant. Enriched pathways were plotted using Python library Matplotlib (Hunter, 2007). The results of enrichment analyses are shown in supplemental data file [Data S8: Metatranscriptome Enrichment Analyses, Related to Figures 3 and 4 and STAR Methods section: Metatranscriptome Enrichment Analyses](#). Heatmaps of all genes in enriched or depleted pathway categories were visualized using the Metaboanalyst 4.0 tools (Chong et al., 2018), with hierarchical gene-level clustering by Pearson similarity and minimum-distance linkage.

Genomic DNA extraction and qPCR

Genomic DNA was extracted from cecal contents using the Zymo Quick-DNA Fecal/Soil Microbe Miniprep Kit (kit# 11-322; Zymo, Irvine, CA) and qPCR was performed using Taqman primers and probes specific for *P. bifementans*, *C. sardiniense* and *C. difficile*

with the conditions as described ([Abdel-Gadir et al., 2019](#); [Bucci et al., 2016](#)) on a QuantStudio 12K Flex Real time PCR system (Applied Biosystems, Beverly, MA). Samples were run in triplicate and compared against standard curves of known biomass of each organism spiked into germfree cecal contents and then extracted to provide normalized CFU counts per gram of cecal contents.

***Clostridium scindens* Stickland reductase gene analysis**

The genomes of *C. scindens* ATCC35704 (GenBank: NZ_CP036170), VE202-05 (GenBank: GCA_000471845.1), MSK 1.16 (RefSeq: GCF_013304115.1), and MGYG-HGUT-013-3 (RefSeq: GCF_902373645.1) were interrogated by protein and nucleotide BLAST with each of the full length coding regions from the *C. difficile* ATCC43255 and *P. bifermentans* DSM14991 proline reductase (*prd* genes) ([Bouillaut et al., 2013](#); [Jackson et al., 2006](#)), glycine reductase (*grd* genes) ([Andreesen, 1994](#); [Berges et al., 2018](#)), and reductive leucine pathway genes (*had* operon genes) ([Kim et al., 2006](#)). Putative orthologs with >80% identity and >80% query coverage were evaluated further. *C. scindens* orthologs, if present, were aligned with the corresponding regions in *C. difficile* and *P. bifermentans* using the PATRIC multi-sequence alignment tool ([Wattam et al., 2017](#)). Aligned regions are shown in [Figure S4: Stickland reductase genetic loci in *C. difficile*, *P. bifermentans* and *C. scindens*](#), Related to [STAR Methods](#) section: [Clostridium scindens Stickland reductase gene analysis](#).

QUANTIFICATION AND STATISTICAL ANALYSIS

Numbers of mice or experimental replicates studied are noted in the figures, associated figure legends, and/or [STAR Methods](#) sections. Complete details of statistical analysis can be found in the associated figure legends and/or [STAR Methods](#) sections.